4.2.1.2 1/3.5 Scale Test

1) Objectives

The ACC design uses an anti-vortex cap at the top of the standpipe to prevent the formation of a vortex as the flow drains from the tank such that the flow will only switch from a high flow to a lower flow when the level in the ACC drops below the top of the standpipe.

Without the anti-vortex cap it is possible for supercritical flow to form at the standpipe inlet as the water level approaches the top of the standpipe. Under these conditions and gas could be entrained, and the flow rate would not switch smoothly. The purpose of these experiments was to demonstrate that the inclusion of the anti-vortex cap will promote smooth flow switching as the tank water level decreases.

The test was conducted to confirm the flow behavior and potential for vortex formation in the ACC and to confirm the effect of the anti-vortex cap.

2) Test Apparatus

The outline drawing of the test facility is shown in Fig. 4.2.1.2-1. The test apparatus consists of the standpipe, test tank, pump, and piping. The anti-vortex cap that is installed at the top of the standpipe was made of transparent acrylate such that the flow can be observed at the standpipe inlet. The scale of the standpipe inlet is 1/3.5 of the actual standpipe design.

Fig. 4.2.1.2-1 Outline Drawing of 1/3.5 Scale Test Apparatus

3) Testing Method

(1) The experiment was scaled using the Froude Number as the basis since there was an open tank with a fluid surface. The relationship between the model tank (*m*) and the actual accumulator (*p*) is given below assuming the Froude Number is defined as

$$Fr = \frac{V}{(g \cdot L)^{0.5}} \quad (4\text{-}1)$$

And $$Fr_p = Fr_m \quad (4\text{-}2)$$

$$Q_p = \left(\frac{L_p}{L_m}\right)^{2.5} \cdot Q_m \quad (4\text{-}3)$$

$$V_p = \left(\frac{L_p}{L_m}\right)^{0.5} \cdot V_m \quad (4\text{-}4)$$

$$t_p = \left(\frac{L_p}{L_m}\right)^{0.5} \cdot t_m \quad (4\text{-}5)$$

where

Fr	:	Froude number
L	:	Typical dimension
Q	:	Typical flow rate
V	:	Typical velocity
t	:	Time
p	:	Subscript denoting the actual ACC
m	:	Subscript denoting the 1/3.5 scale model

(2) The flow rate was measured by an ultrasonic flow meter and the tank water level was measured by the level marking on the sidewall of the tank.

4) Test Conditions

The test conditions are shown in Table 4.2.1.2-1. Two types of standpipe inlet (with the anti-vortex cap and without it) were tested. The tests were performed using two flow rates in which the test and actual ACC Froude numbers were preserved. The flow rates were [ ] and [ ]. These cover the expected flow rates at flow switching for minimum and maximum initial gas pressures, respectively. The injection characteristics with test flow rates are shown in Figs. 4.2.1.2-2 to 4.2.1.2-5.

Table 4.2.1.2-1 Test Conditions

Test Number	Test Condition			Remarks	Corresponding Actual Condition	
	Anti-vortex Cap	Flow Characteristics	Flow Rate just before switching (gpm (l/sec))		Initial Gas Pressure (psig (MPa(g)))	Flow Rate just before switching (gpm (m^3/h))
1-1	No	Fig. 4.2.1.2-2	[ ]	Froude number is preserved.	[ ]	[ ]
1-2	Yes	Fig. 4.2.1.2-3	[ ]			[ ]
2-1	No	Fig. 4.2.1.2-4	[ ]		[ ]	[ ]
2-2	Yes	Fig. 4.2.1.2-5	[ ]			[ ]

5) Parameters and Measuring Equipment

Flow rate and water level were measured to confirm the conditions during flow switching. The flow rate was measured using an ultrasonic flow meter and the tank water level was measured by the level markings on the sidewall of the tank.

6) Test Results and Consideration

Test results are summarized in Table 4.2.1.2-2. The flow at the inlet for various conditions is shown in Photos. 4.2.1.2-1(1/2), (2/2) through 4.2.1.2-2(1/2), (2/2). The following observations were made during the test.

(1) In the case of the standpipe inlet without the anti-vortex cap, a slight surface dimple appeared above the inlet and the initiation of supercritical flow developed when the water level began to decrease. When the water level decreased further, the supercritical flow condition was apparent and the surface dimple reached into the standpipe, and gas entrainment occurred. (Photo. 4.2.1.2-1(1/2), (2/2))

(2) Below the water level where the supercritical flow condition becomes apparent, the critical depth became smaller consistent with the water level reduction. This resulted in a lower flow rate and a slower reduction of the water level.

(3) The condition described in (2) above is apparent in the wave pattern. For example, in Fig. 4.2.1.2-2, supercritical flow was apparent, gas entrainment started 26 seconds after initiation of the test, and the variation of the flow rate became lager. As the flow rate became smaller, it took as long as 5 seconds before the flow rate into the standpipe became zero.

(4) This qualitative condition appeared in the case of both the minimum initial gas pressure of [ ] and the maximum initial gas pressure of [ ] without any significant differences.

(5) In the case of the standpipe inlet with the anti-vortex cap, a slight disturbance appeared on the water surface as the water level decreased from just above the upper end of the cap to the lower end of the cap. However, neither a vortex nor a supercritical flow occurred, and the flow rate switched sharply over a short period of time. (Photos. 4.2.1.2-2(1/2), (2/2))

This condition is apparent in the wave pattern. For example, in Fig. 4.2.1.2-3, the flow rate into the standpipe became zero in approximately 1 second. The flow rate switched much more quickly than the case without the anti-vortex cap (which was approximately 5 seconds in Fig. 4.2.1.2-2).

(6) Based on the data and visual observations described above, the desired effects of the anti-vortex cap were confirmed.

Table 4.2.1.2-2 Summary of Test Results

Test Number (T. No)	Test Condition		Test Results		
	Flow Characteristics	Anti-vortex Cap	Vortex Formation	Time to finishing switching (sec)	Remark
1-1	Fig. 4.2.1.2-2	No	Yes	Approx. 5	Photo. 4.2.1.2-1 (1/2), (2/2)
1-2	Fig. 4.2.1.2-3	Yes	No	Approx. 1	Photo. 4.2.1.2-2 (1/2), (2/2)
2-1	Fig. 4.2.1.2-4	No	Yes	[ ]	-
2-2	Fig. 4.2.1.2-5	Yes	No	[ ]	-

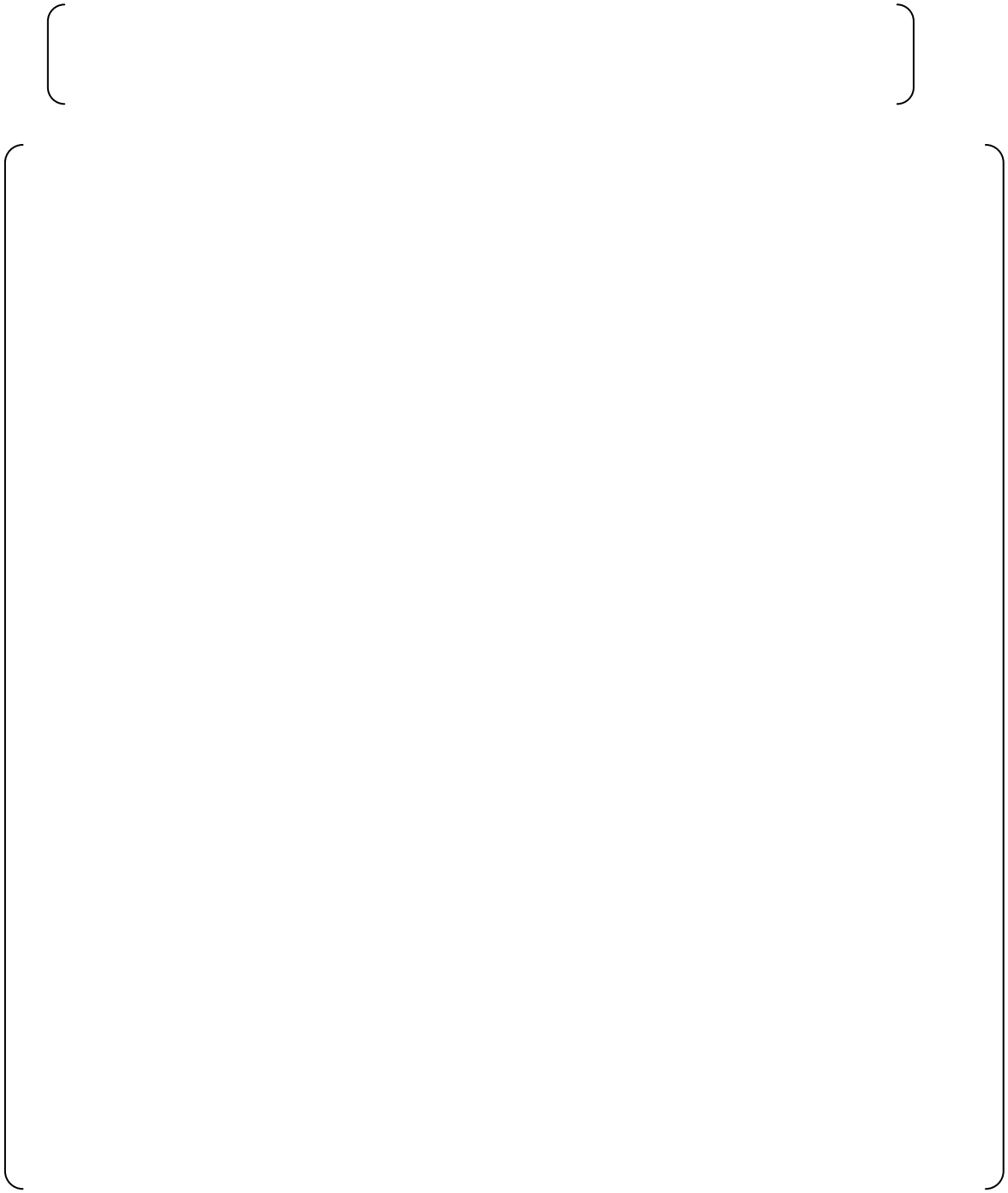

Photo. 4.2.1.2-1 (1/2) Visualization of Flow without Anti-Vortex Cap (T. No. 1-1) 1/2

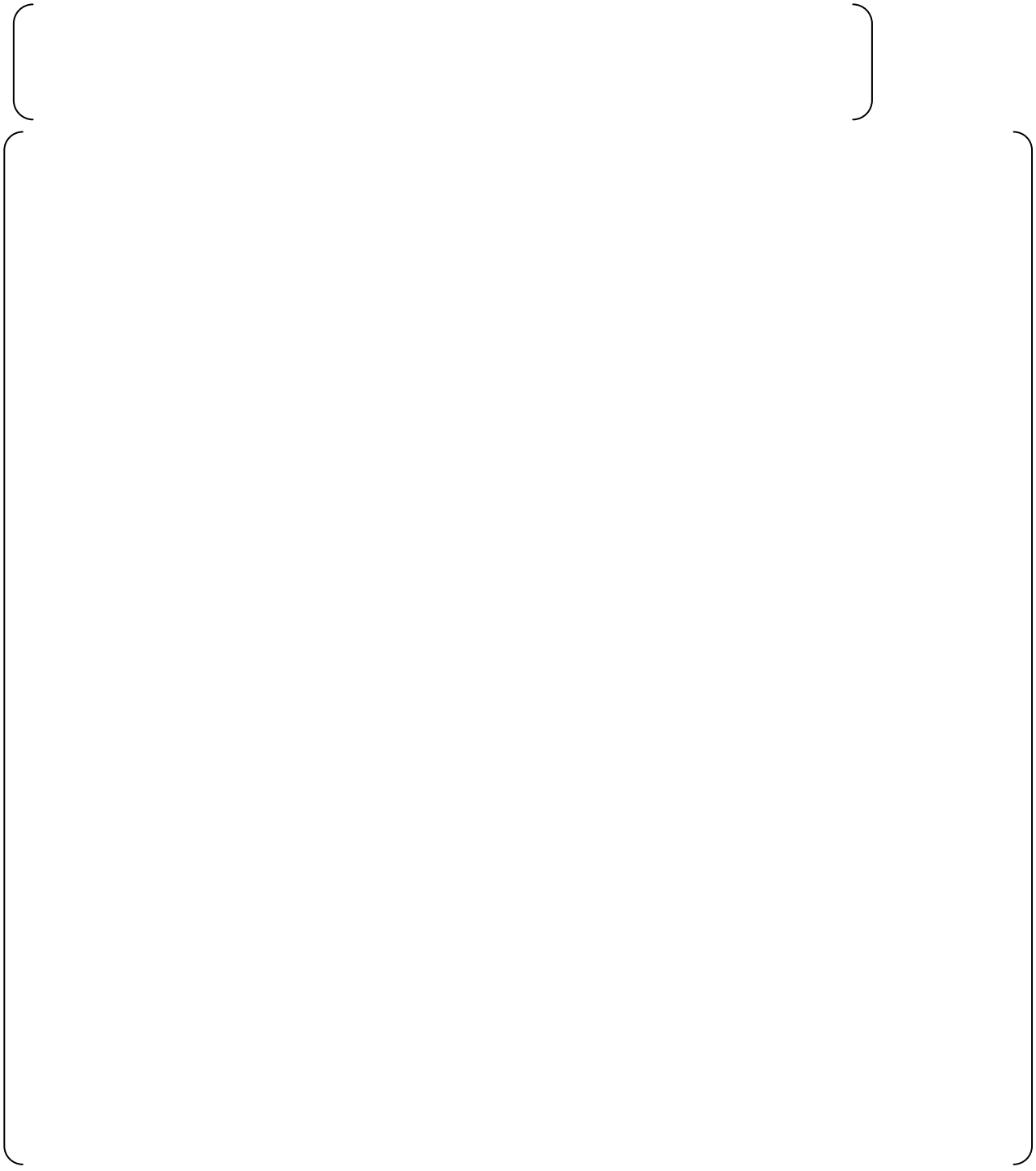

Photo. 4.2.1.2-1 (2/2) Visualization of Flow without Anti-Vortex Cap (T. No. 1-1) 2/2

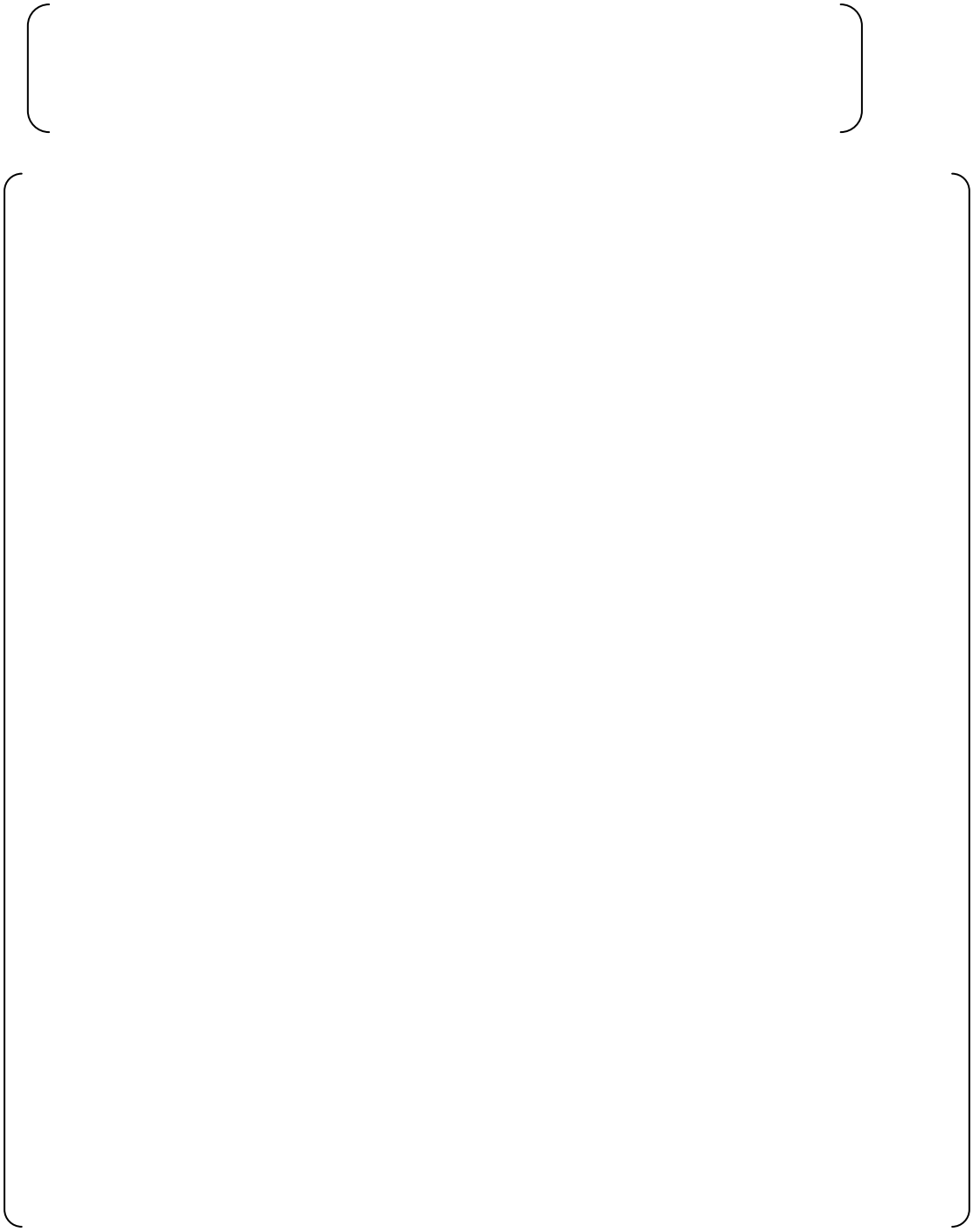

Photo. 4.2.1.2-2 (1/2) Visualization of Flow with Anti-Vortex Cap (T. No. 1-2) 1/2

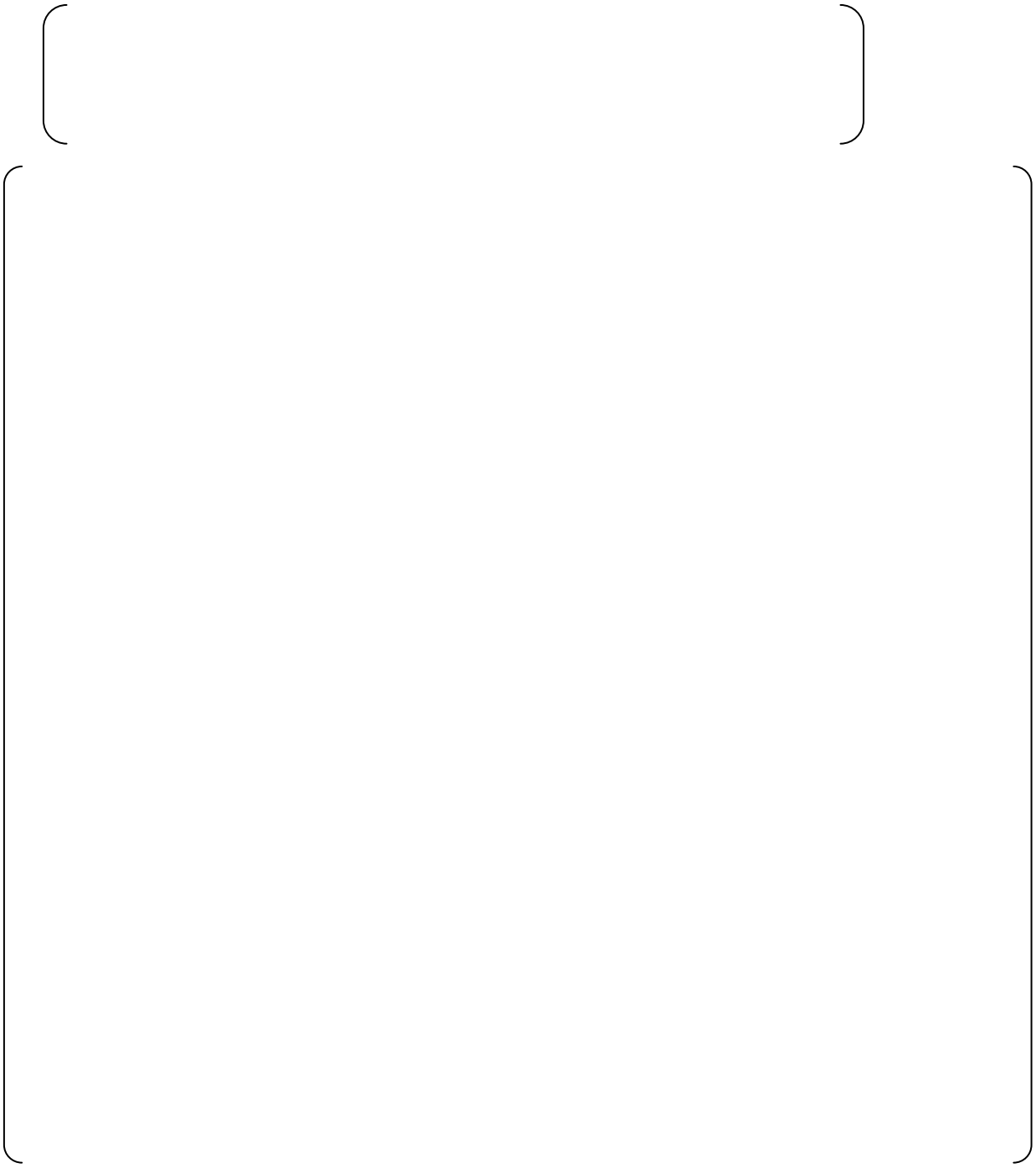

Photo. 4.2.1.2-2(2/2) Visualization of Flow with Anti-Vortex Cap (T. No. 1-2) 2/2

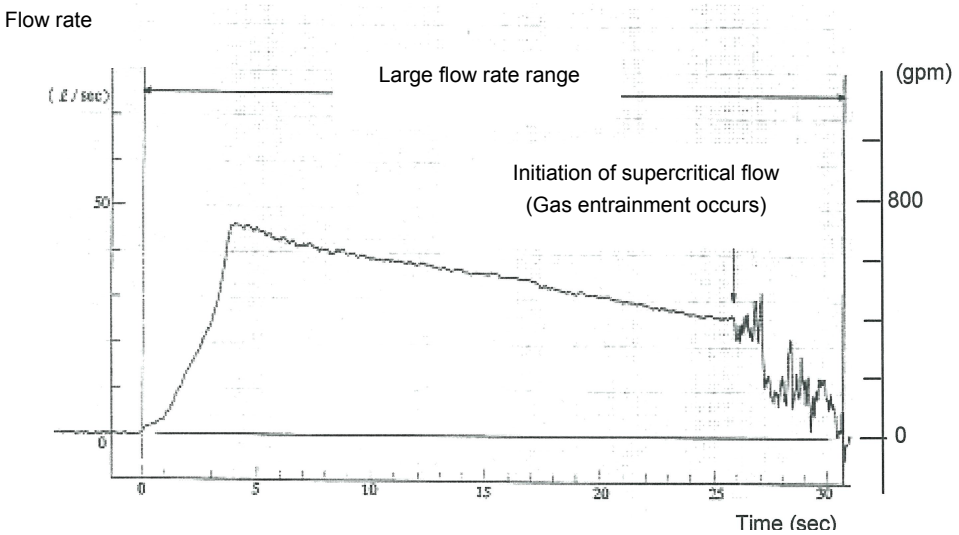

Fig. 4.2.1.2-2 Test Flow Characteristics without Anti-Vortex Cap (T. No. 1-1)

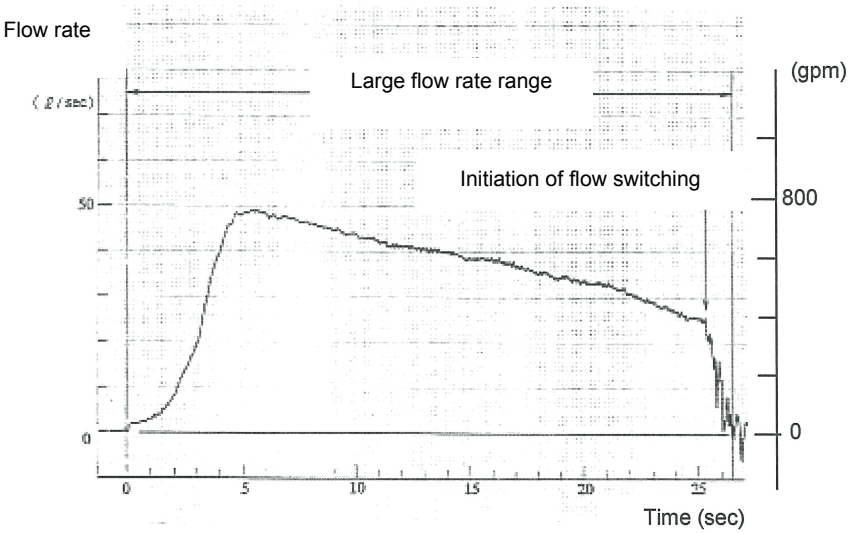

Fig. 4.2.1.2-3 Test Flow Characteristics with Anti-Vortex Cap (T. No. 1-2)

Fig. 4.2.1.2-4 Test Flow Characteristics without Anti-Vortex Cap (T. No. 2-1)

Fig. 4.2.1.2-5 Test Flow Characteristics with Anti-Vortex Cap (T. No. 2-2)

4.2.1.3 1/5-Scale Test

1) Objectives

The objective of 1/5-scale test was to observe the flow in the flow damper during large and small flow, large to small flow switching, and to confirm the expected behavior of the flow.

2) Test Apparatus

The outline drawing of the test apparatus is shown in Fig. 4.2.1.3-1. The test facility consists of a test tank, flow damper, standpipe, injection piping, and exhaust tank. The flow damper is made of transparent acrylate to allow the fluid characteristics in the flow damper to be observed. A ball valve (nominal diameter is [ ]) is provided in the injection line as the isolation valve and a gate valve (nominal diameter is [ ]) is also provided in the injection line to control the flow resistance.

Fig. 4.2.1.3-1 Outline Drawing of the Visualization Test Apparatus

The specifications of the test facility are as follows:

(1) Test tank

Design Pressure	:	[ ]
Diameter	:	[ ]
Height	:	[ ]
Volume	:	[ ]

(2) Flow damper and standpipe (1/5-scale actual size)

Diameter of vortex chamber	:	[ ]
Height of vortex chamber	:	[ ]
Shape of standpipe	:	[ ]

(3) Injection piping

Inner diameter (Simulating the pressure drop)	:	[ ]

(4) Exhaust tank

Design Pressure	:	[ ]
Diameter	:	[ ]
Height	:	[ ]
Volume	:	[ ]

3) Testing Method

(1) Visualization tests were conducted for three cases: (i) examining flow characteristics during large flow injection and flow switching by setting the initial pressure at [ ], which is the maximum design pressure of the test tank; (ii) examining flow characteristics during small flow injection by setting the initial pressure at [ ] for an extended small flow injection time, and (iii) examining flow characteristics during flow switching by setting the initial pressure at [ ], which has the same Froude number as that of the actual plant condition.
(2) The flow characteristics in the flow damper were recorded and observed using a video camera, as shown in Fig. 4.2.1.3-1.
(3) The characteristics of the flow in the vortex chamber were observed using blue ink as a flow tracer.

4) Test Conditions

Visualization test conditions are shown in Table 4.2.1.3-1.

Table 4.2.1.3-1 Visualization Test Conditions

5) Parameters and Measuring Equipment

Pressure, water level, and temperature were measured to calculate cavitation factors and flow rate coefficients. The differential pressure transducer for measuring water level in the tank and the attachments for the pressure transducer are shown in Fig. 4.2.1.3-1.

6) Test Results and Consideration

The visualization test results are summarized in Table 4.2.1.3-2 and the flow in the vortex chamber during large flow, large/small flow switching, and small flow are shown in Photos. 4.2.1.3-1 to 4.2.1.3-3. The white lines are added in the photos to clearly show the tracer trajectories.

(1) The characteristics of the large flow are shown in Photo. 4.2.1.3-1. Since the flow tracer traveled from the point of the flow from the standpipe directly to the flow damper exit following collision with the water from the small flow inlet, it was confirmed that a vortex was not formed in the vortex chamber during large flow injection.

(2) The characteristics of the large / small flow switching are shown in Photo. 4.2.1.3-2. It shows the beginning of the formation of a vortex during flow rate switching. It was also confirmed that gas entrainment from the standpipe did not occur and the flow rate switched smoothly in a short time.

(3) The characteristics of small flow are shown in Photo. 4.2.1.3-3. It was confirmed that the flow tracer swirled to the outlet, and a stable vortex was formed in the vortex chamber. No cavitation was observed at the center of the vortex.

Table 4.2.1.3-2 Visualization Test Results

Test Number (T. No.)	Initial Pressure (Test Tank)	Large Flow	Flow Rate Switching	Small Flow
1/5-1	[ ] [ ]	A vortex was not formed in the vortex chamber during large flow.	The flow rate switched smoothly in a short time.	-
1/5-2	[ ] [ ]	-	-	A stable vortex was formed in the vortex chamber.
1/5-3	[ ] [ ]	-	The flow rate switched smoothly in a short time.	-

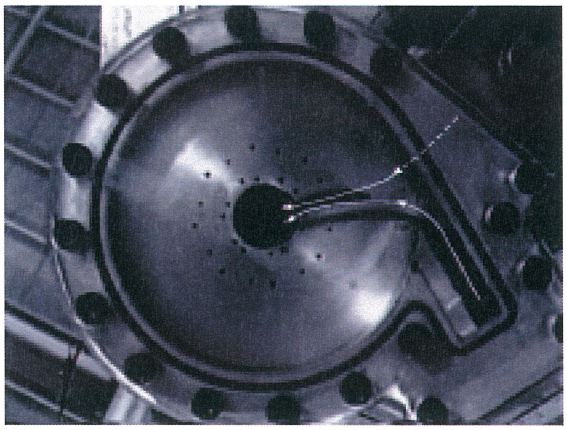

Photo. 4.2.1.3-1 Large Flow

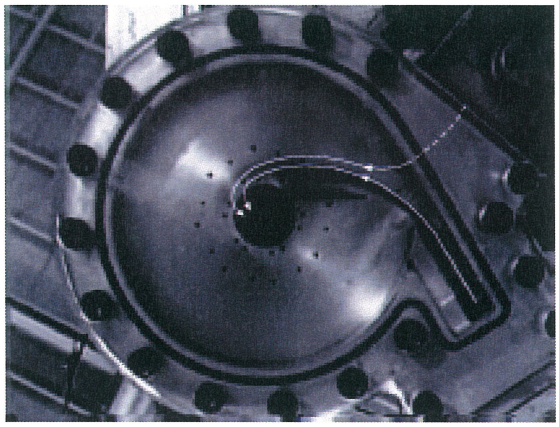

Photo. 4.2.1.3-2 Switching Flow Rate

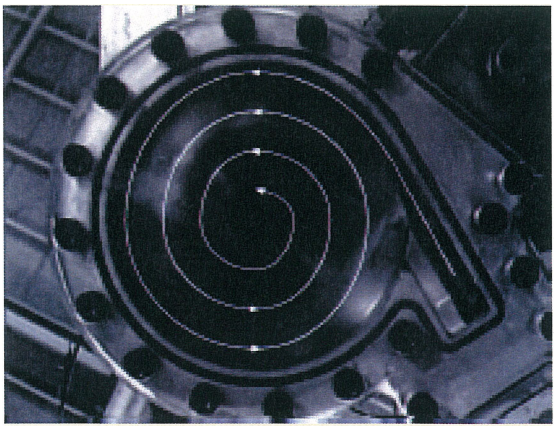

Photo. 4.2.1.3-3 Small Flow

4.2.2 Qualification Testing

1) Objectives

(1) Verification of performance during large flow and small flow phases:
Tests were conducted to confirm that the performance of the flow damper, during large flow and small flow respectively, met the acceptance criteria (resistance coefficient for large and small flow injection).

(2) Verification of the flow switching without need of any moving parts:
It was assumed that the injection flow rate shifts from large flow to small flow when the tank water level decreases to the lower edge of the standpipe anti-vortex cap. This design feature was verified by actual injection testing.

(3) Confirmation of the effect of dissolved nitrogen gas:
Since the accumulator utilizes compressed nitrogen gas, nitrogen gas may dissolve in the water. If the water in the accumulator contains dissolved nitrogen gas, it is assumed that the gas comes out of solution and affects the flow characteristics of the flow damper. Therefore, tests were conducted with nitrogen-rich water to confirm that the effect of nitrogen gas did not impact the ACC performance.

2) Test Facility

The schematic and outline drawing of the test facility and the general flow path are shown in Fig. 4.2.2-1 and Fig. 4.2.2-2. The test facility consists of a test tank, flow damper, injection piping, and exhaust tank. The flow damper is installed in the test tank. The test tank and the flow damper are full-scale. A ball valve is provided in the injection line as the isolation valve and a gate valve is provided in the injection line to control flow resistance. A pressure control valve is provided on the upper side of the exhaust tank to control the tank pressure during the test.

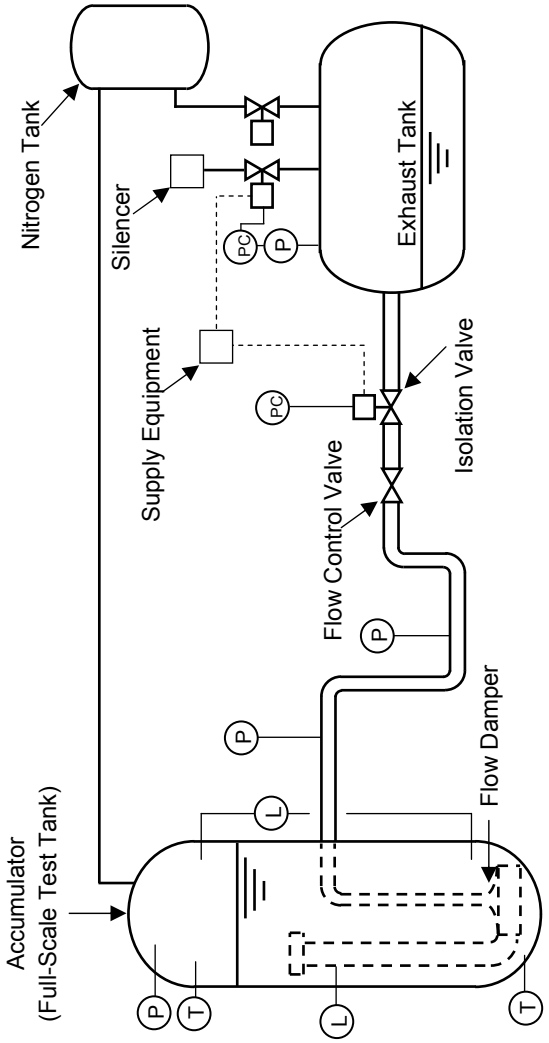

Fig. 4.2.2-1 Schematic Drawing of the Full-Scale Test Facility

Fig. 4.2.2-2 Outline Drawing of the Full-Scale Test Facility

3) Test Conditions

Table 4.2.2-1 Test Conditions of Full-Scale Test

4) Parameters and Measuring Equipment

5) Acceptance Criteria

6) Test Results and Conditions

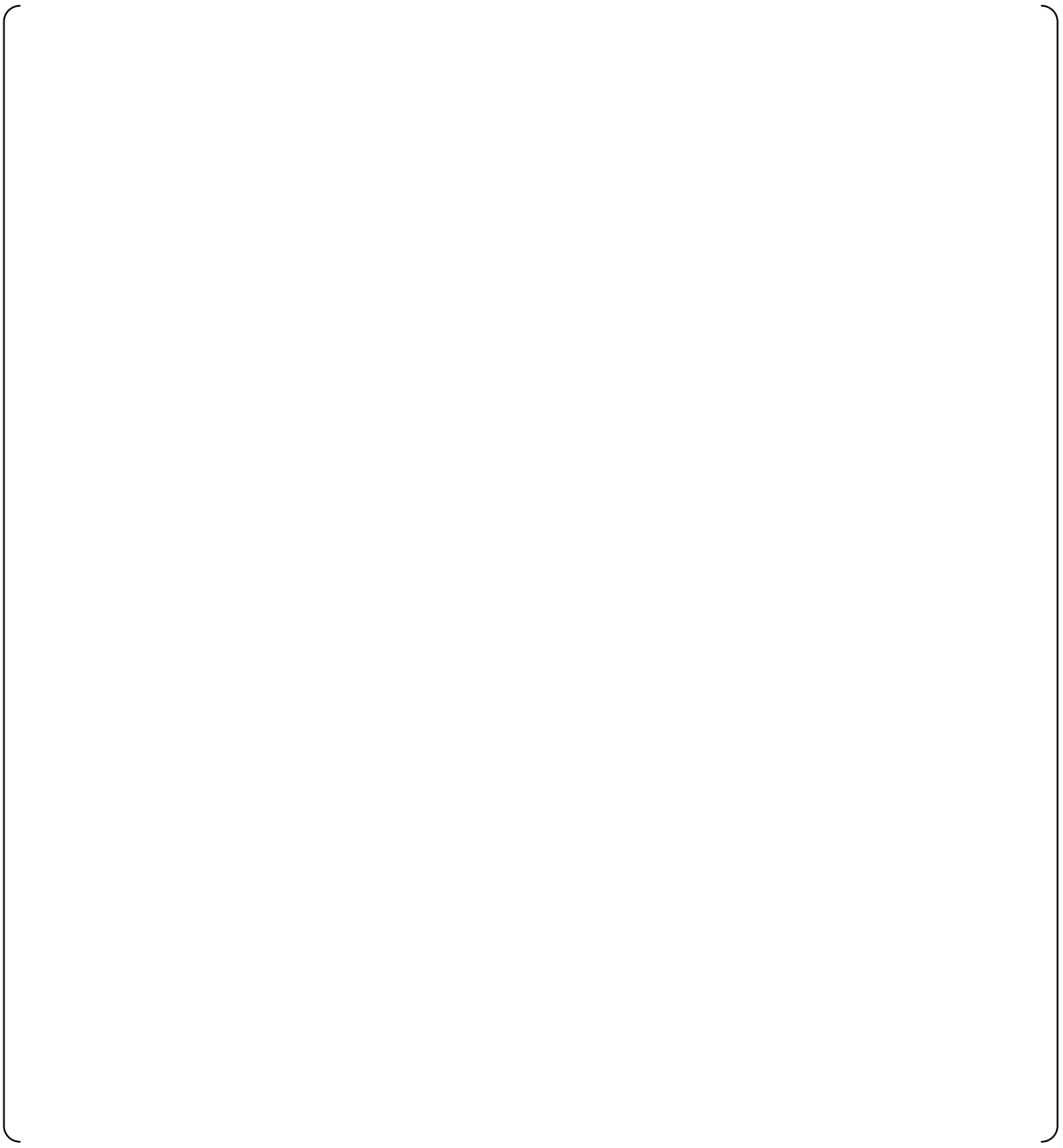

Table 4.2.2-2 Flow Switching Water Level

7) Quality Assurance

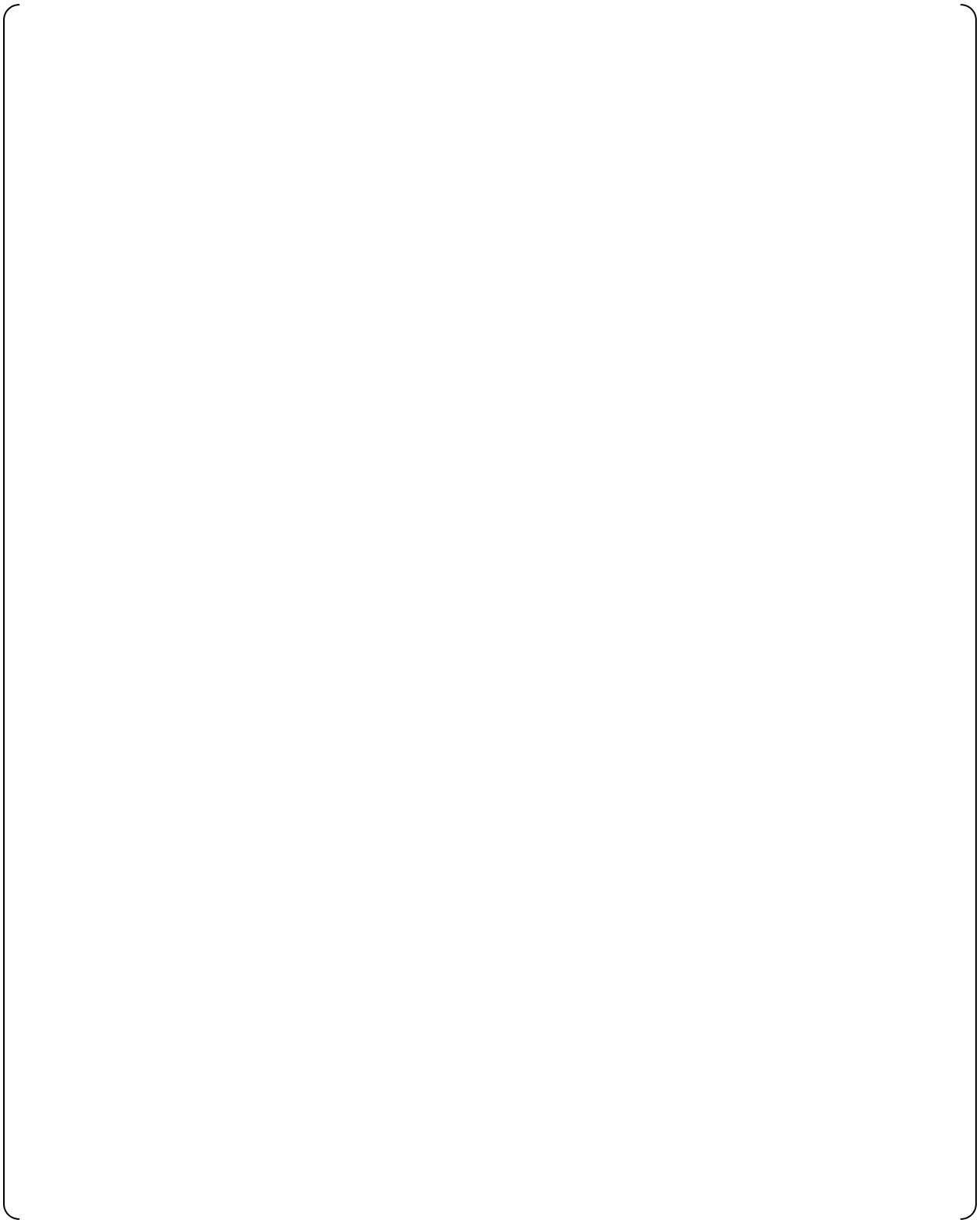

Fig. 4.2.2-3 (1/2) Full-Scale Test Results (Case 1) 1/2

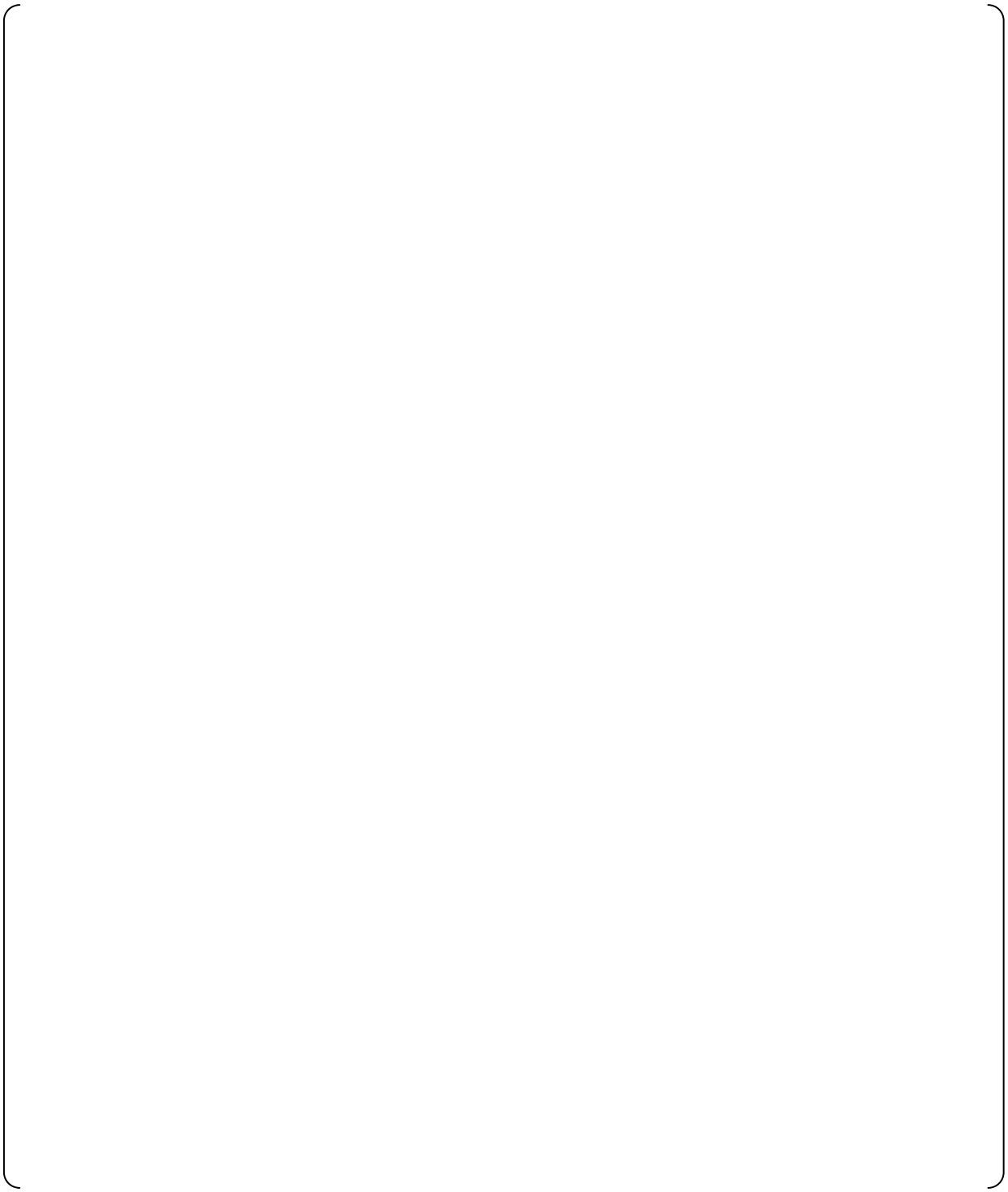

Fig. 4.2.2-3 (2/2) Full-Scale Test Results (Case 1) 2/2

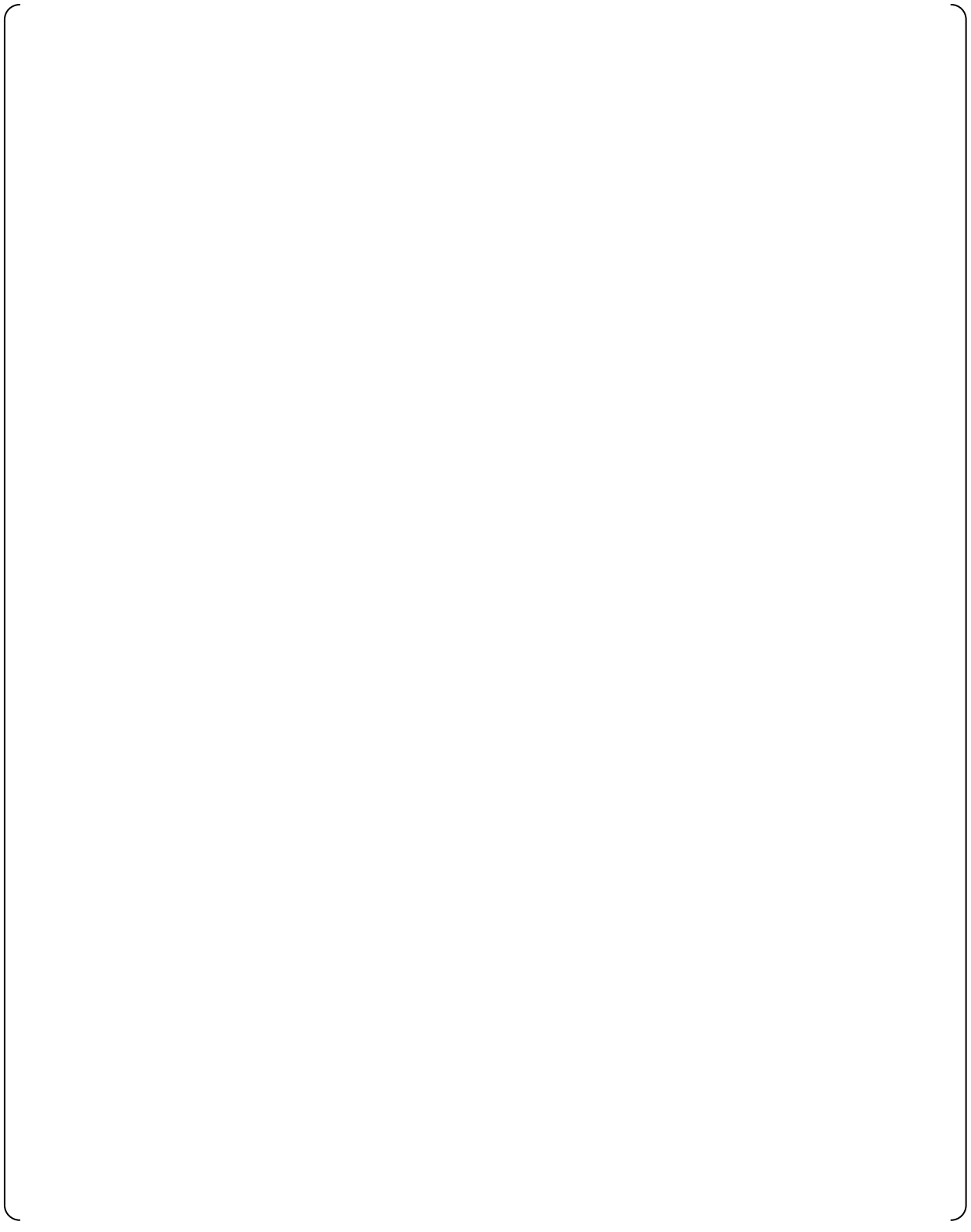

Fig. 4.2.2-4 (1/2) Full -Scale Test Results (Case 2) 1/2

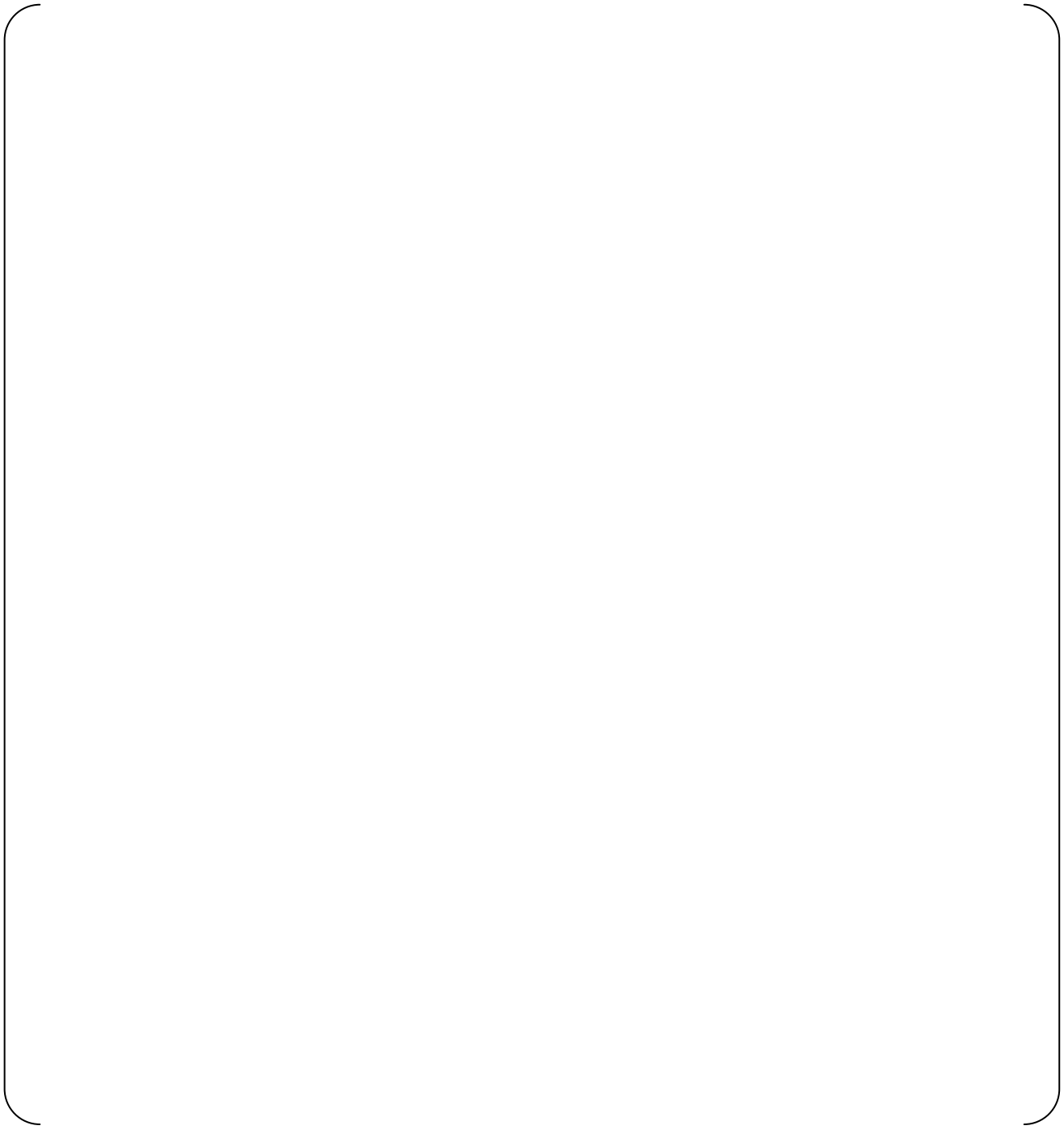

Fig. 4.2.2-4 (2/2) Full-Scale Test Results (Case 2) 2/2

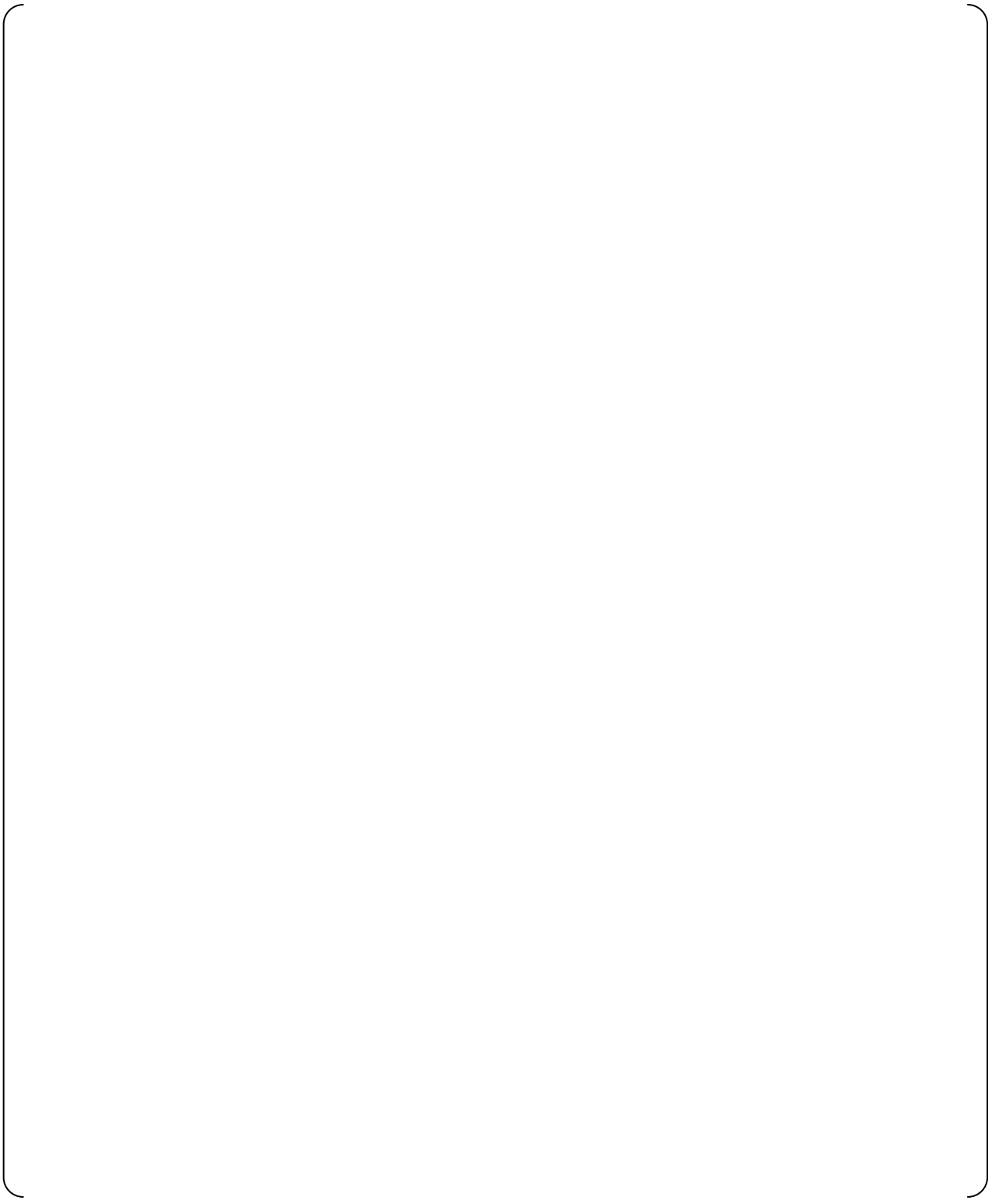

Fig. 4.2.2-5 (1/2) Full-Scale Test Results (Case 3) 1/2

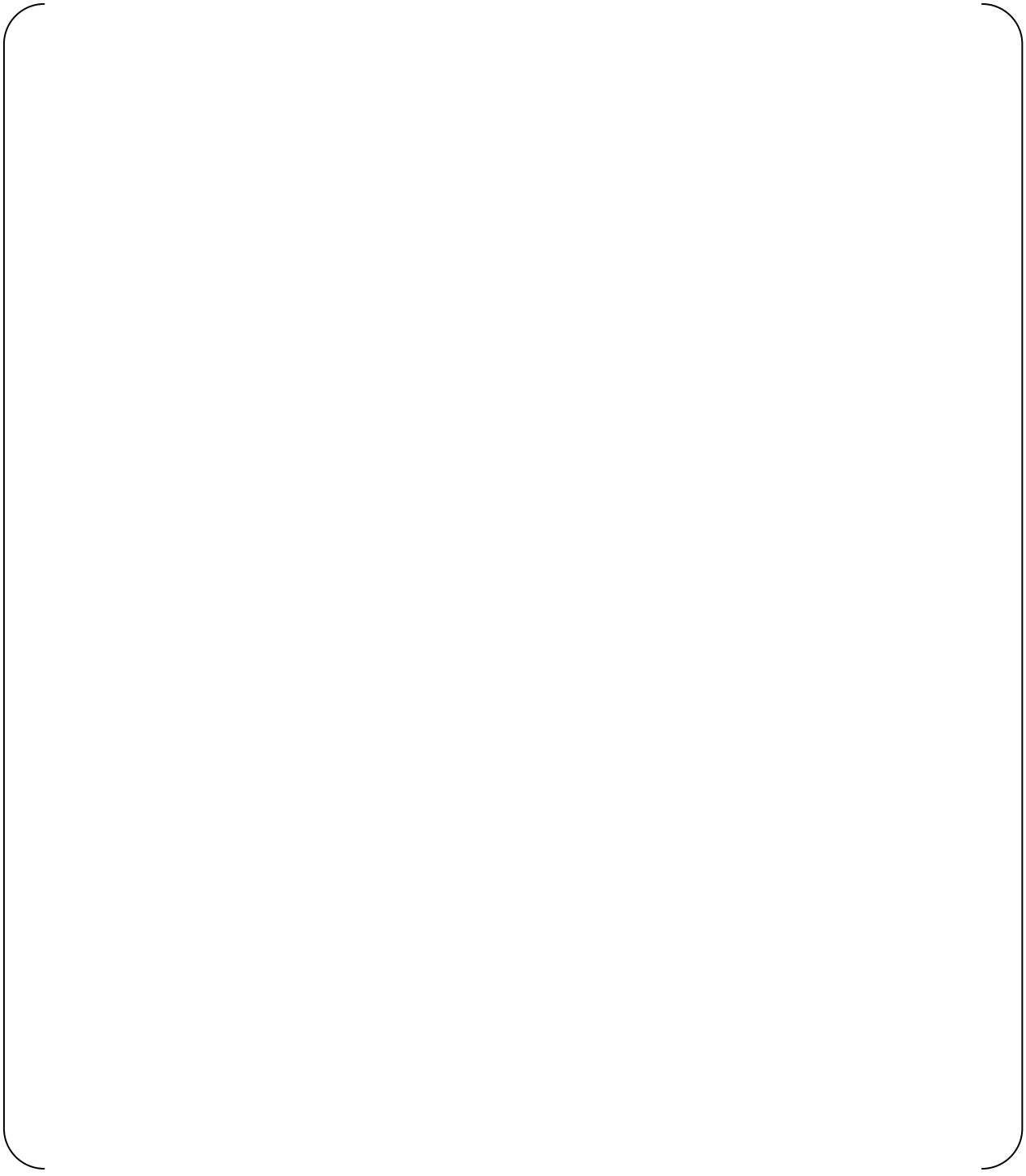

Fig. 4.2.2-5(2/2) Full-Scale Test Results (Case 3) 2/2

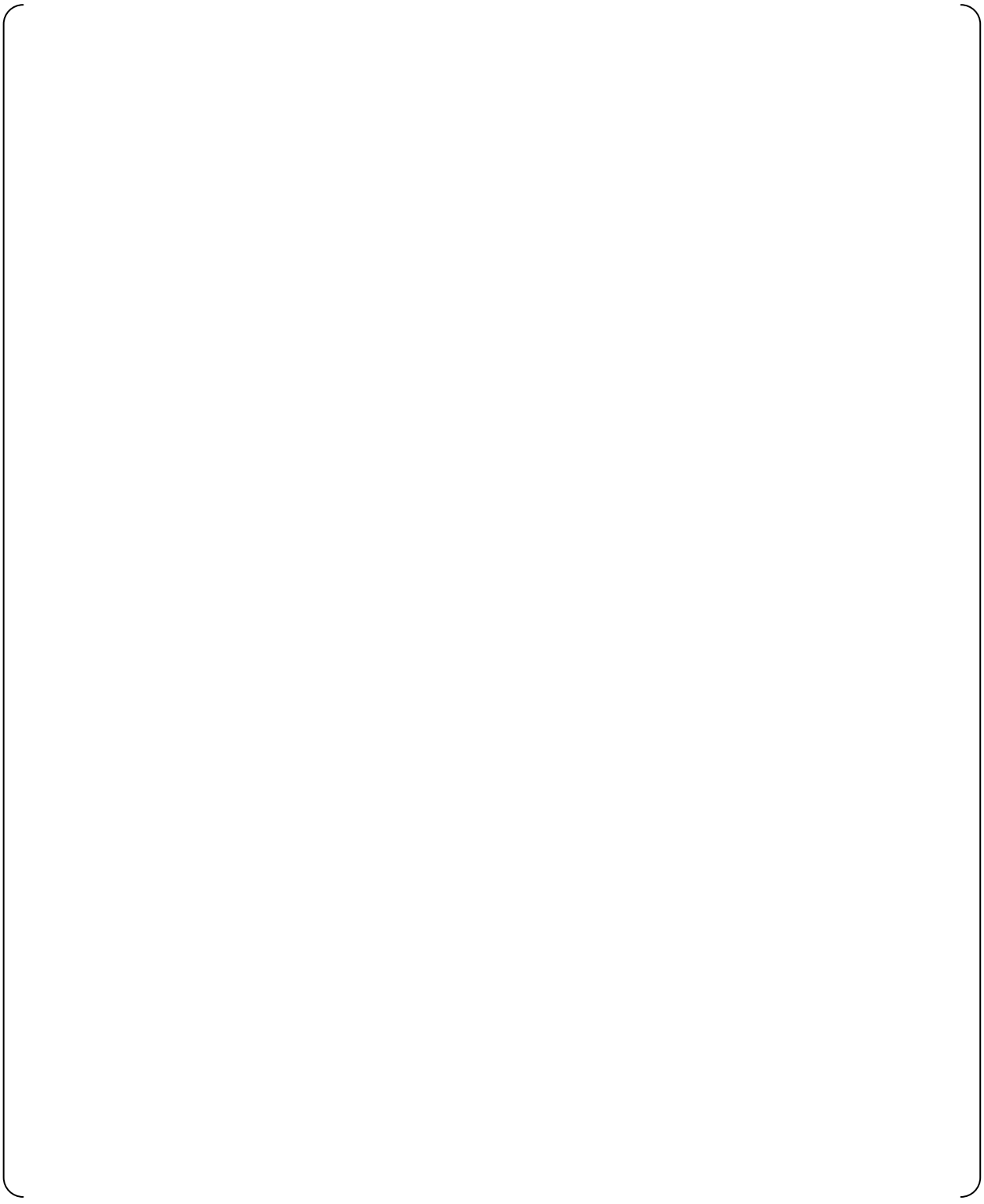

Fig. 4.2.2-6 (1/2) Full-Scale Test Results (Case 4) 1/2

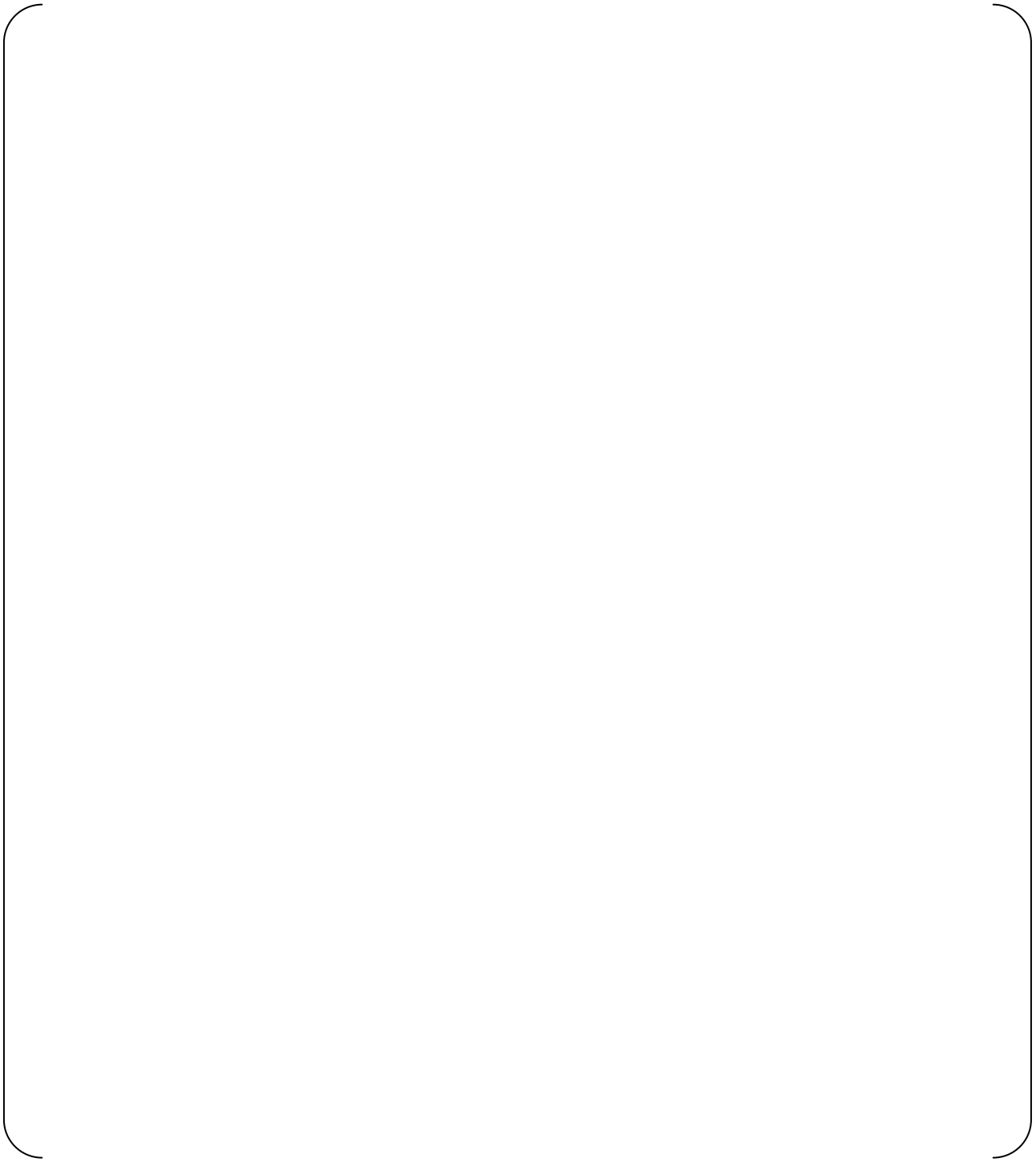

Fig. 4.2.2-6 (2/2) Full-Scale Test Results (Case 4) 2/2

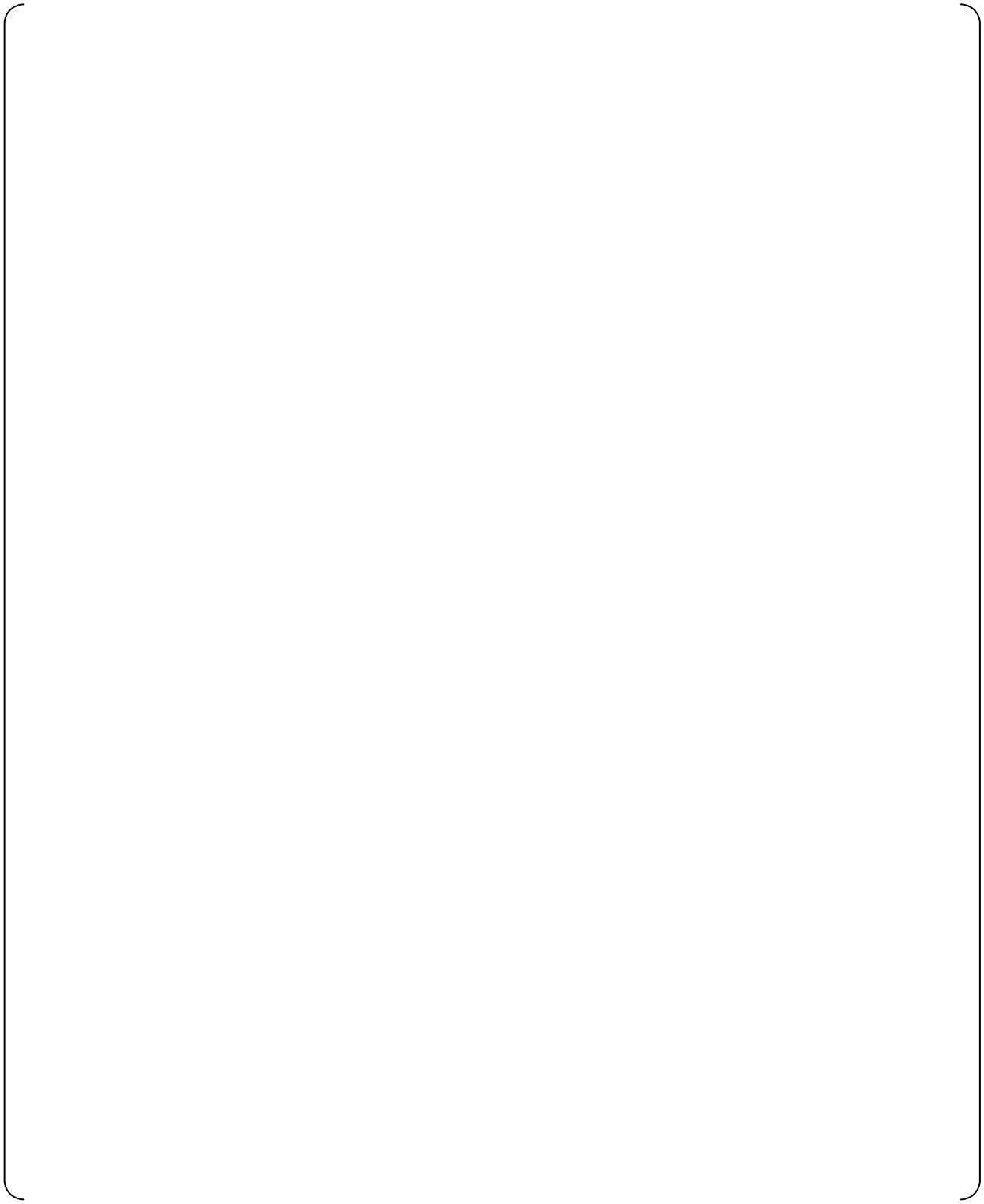

Fig. 4.2.2-7 (1/2) Full-Scale Test Results (Case 5) 1/2

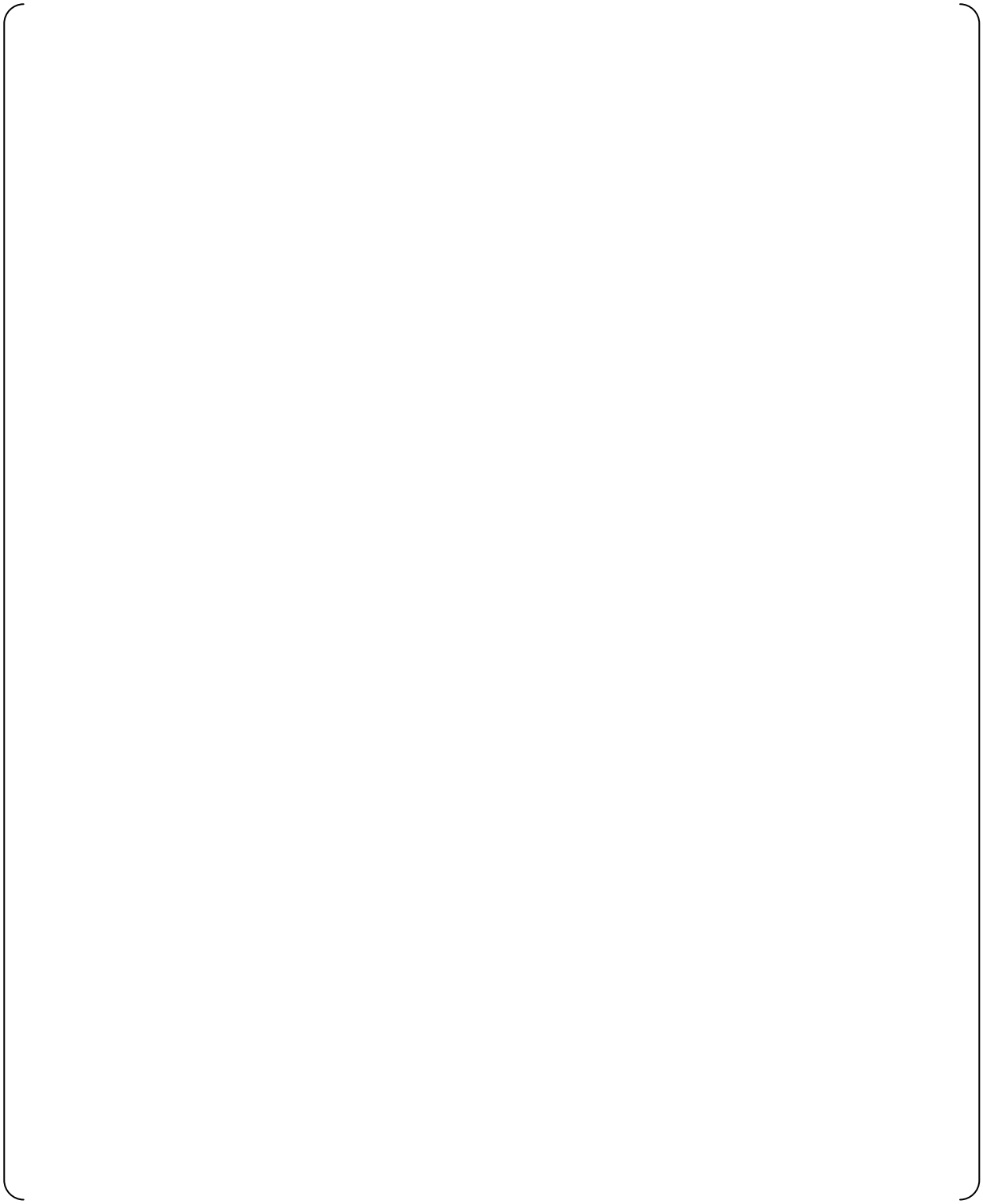

Fig. 4.2.2-7 (2/2) Full-Scale Test Results (Case 5) 2/2

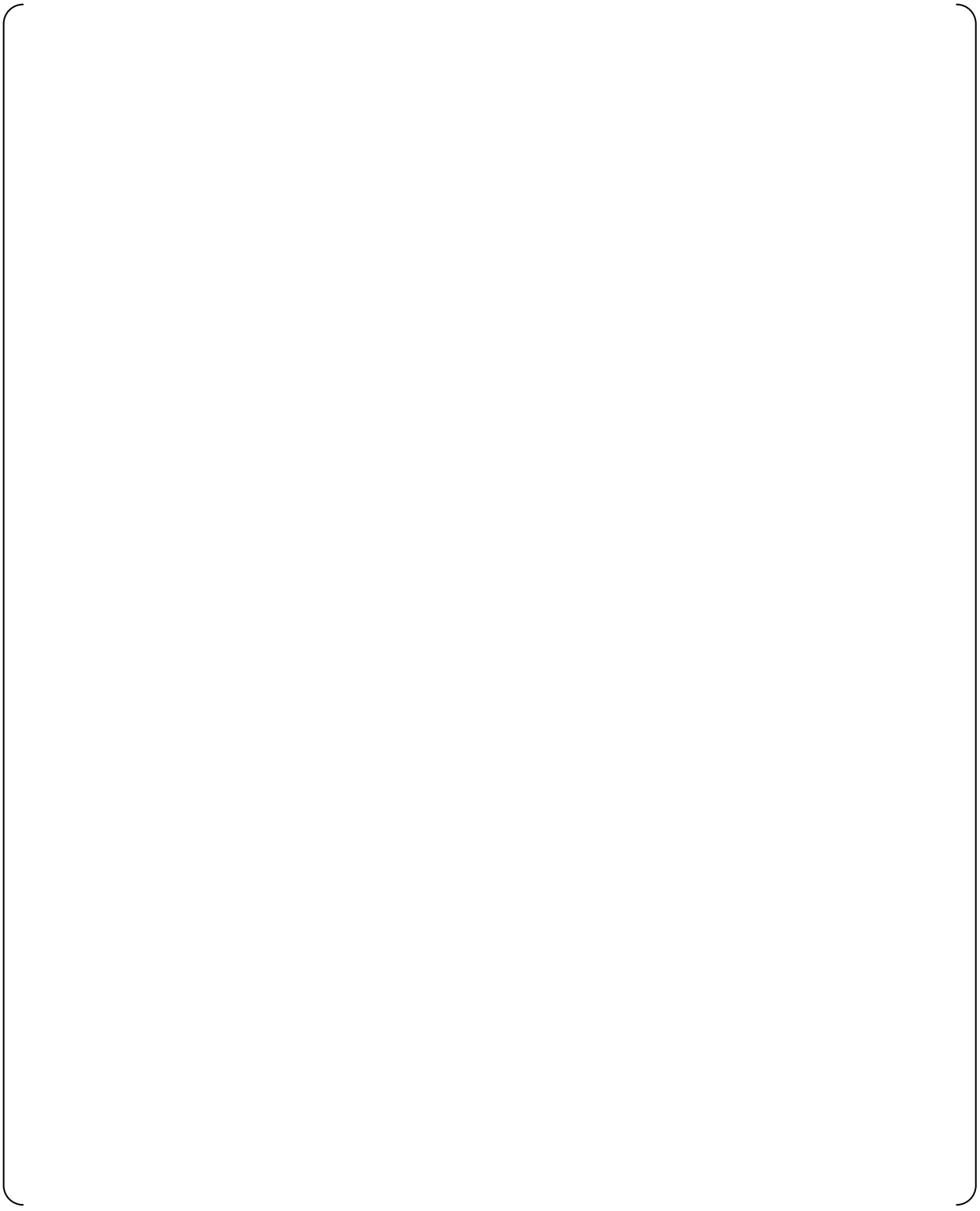

Fig. 4.2.2-8 (1/2) Full-Scale Test Results (Case 6) 1/2

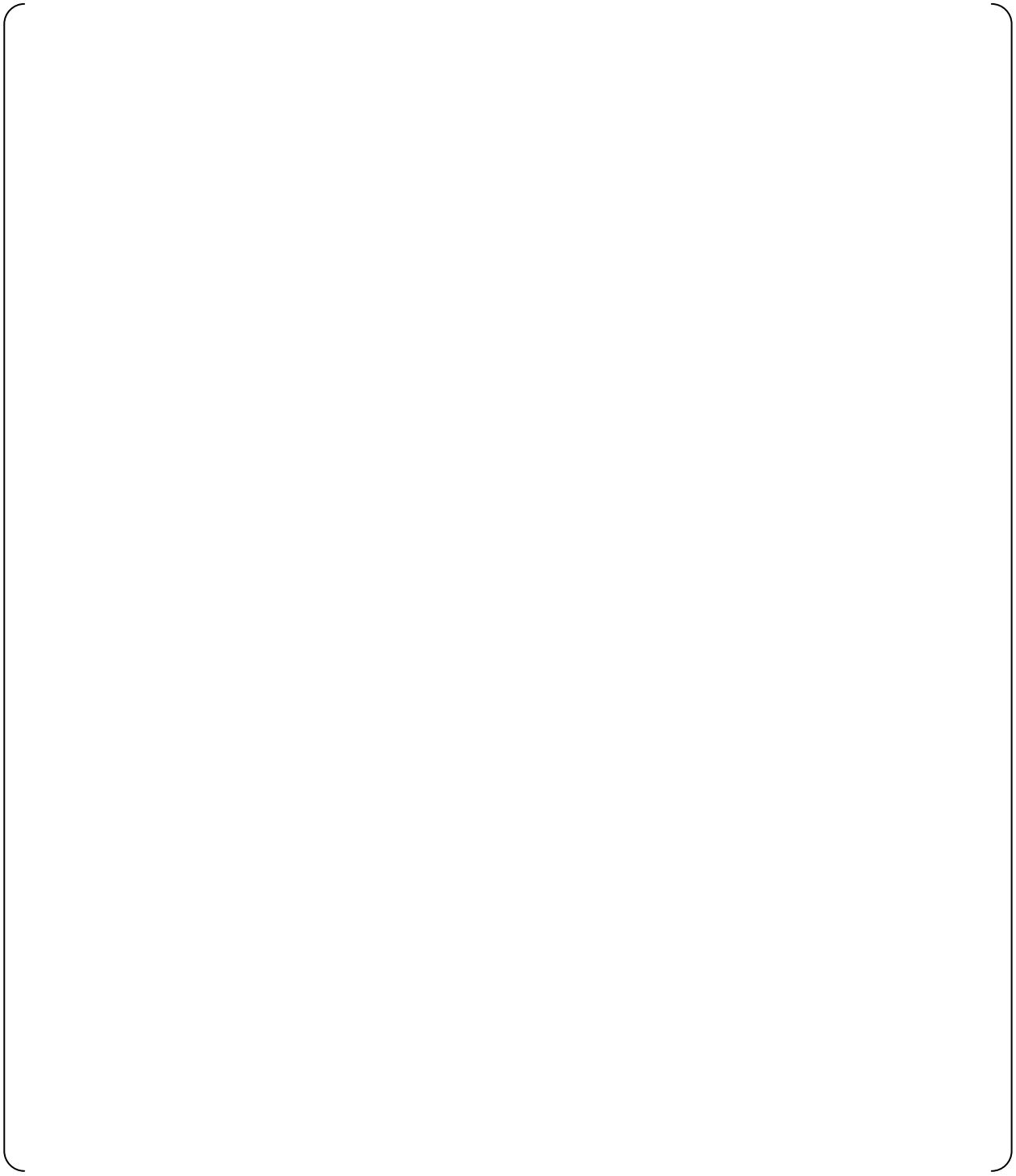

Fig. 4.2.2-8 (2/2) Full-Scale Test Results (Case 6) 2/2

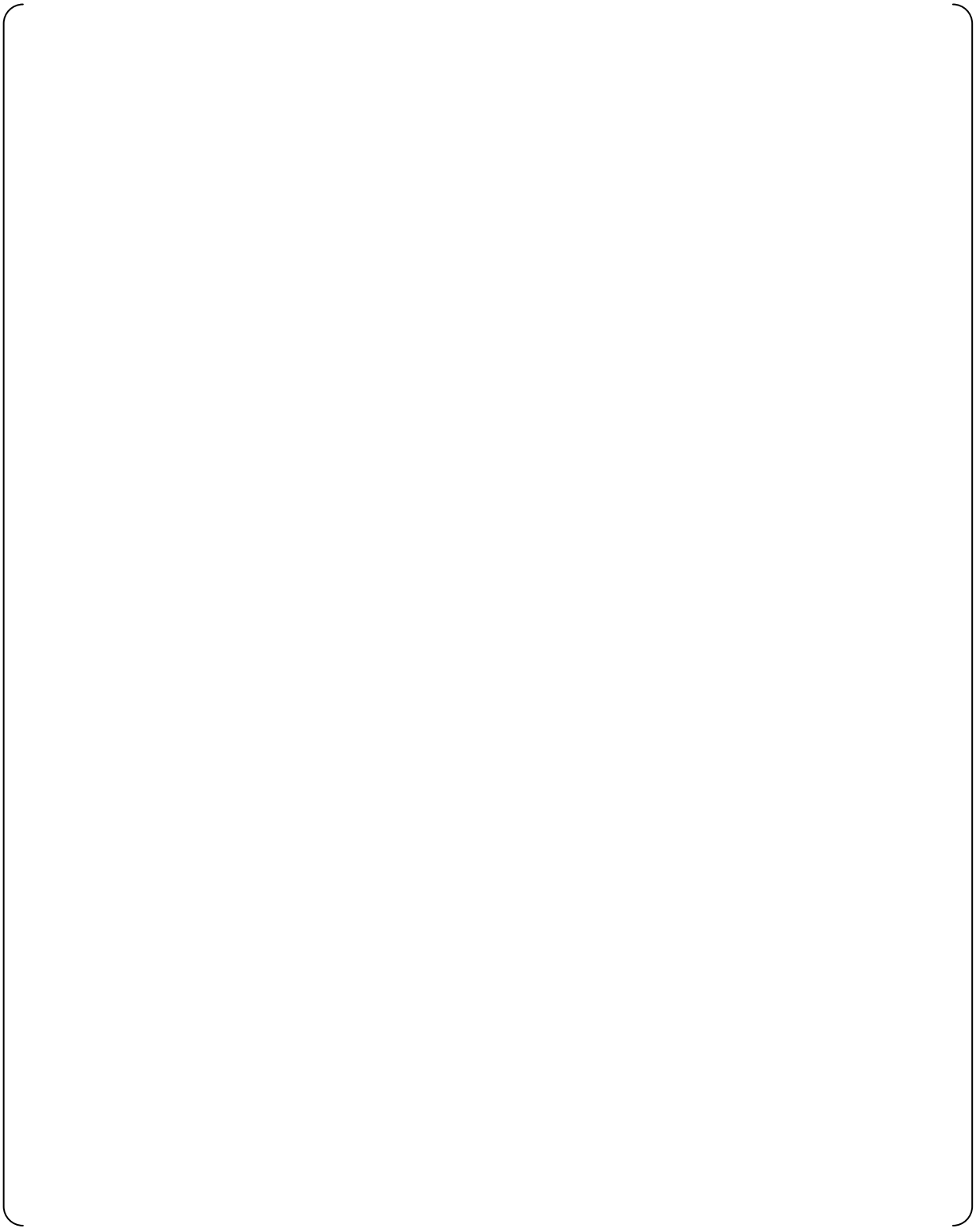

Fig. 4.2.2-9(1/2) Full-Scale Test Results (Case 7) 1/2

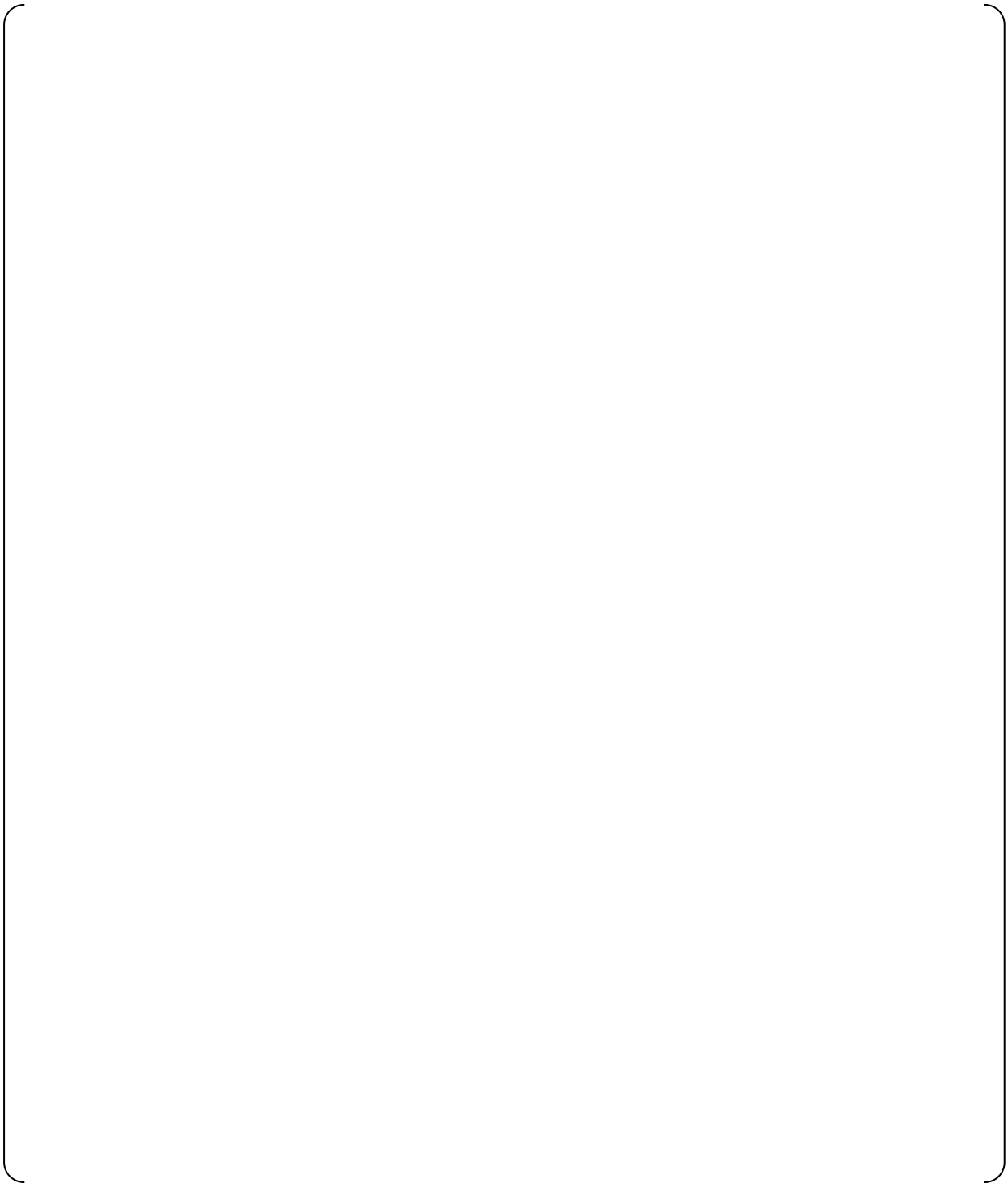

Fig. 4.2.2-9(2/2) Full-Scale Test Results (Case 7) 2/2

5.0 CONCEPT OF THE SAFETY ANALYSIS MODEL

Section 5 describes how to apply the hydraulic performance measured from the full-scale test results to the safety analysis. The accumulator flow rate is modeled in the safety analyses through parameters such as the characteristic equations of the flow damper and its uncertainty, uncertainty of flow rate switching, and the effect of dissolved nitrogen. According to the methodologies outlined below, these parameters are treated appropriately in the safety analyses.

5.1 Flow Rate Characteristics for Safety Analysis

Subsection 5.1 discusses characteristic equations for accumulator flow rates and its uncertainties used in the safety analysis.

5.1.1 Characteristic Equations of Flow Rates for the Safety Analysis

Fig. 5.1-1 The Flow Characteristics of the Flow Damper

5.1.2 Estimation of Uncertainty of the Characteristic Equations of Flow Rates

Table 5.1-1 Dispersion of the Data from the Experimental Equations

Table 5.1-2 Instrument Uncertainties

Table 5.1-3 Total Uncertainty of Flow Rate Coefficient (Experimental Equations) for Safety Analysis of US-APWR

5.2 Estimation of Potential Uncertainties of Water Level for Switching Flow Rates

Table 5.2-1 Uncertainty of Water Level for Switching Flow Rates

5.3 Treatment of Dissolved Nitrogen Gas Effect in the Safety Analysis

5.4 LOCA Analytical Model and Computational Procedure for Characteristic Equations

6.0 CHARACTERISTIC EQUATIONS IN THE PRE-OPERATIONAL TEST

7.0 SUMMARY

The Mitsubishi Heavy Industries, Ltd. Advanced Accumulator (ACC) design will be used in MHI's Advanced Pressurized Water Reactors. The ACC design simplifies the emergency core cooling system design by integrating the short term large flow rate design requirements currently satisfied in conventional pressurized water reactor designs by the combined injection capabilities of the primary system accumulator and the low head safety injection pump into a single passive device, the ACC.

The ACC is a borated water storage tank with a fluidic device that throttles the flow rate of cooling water injected into a reactor vessel from a large to a small flow rate. A conceptual drawing of the ACC is shown below.

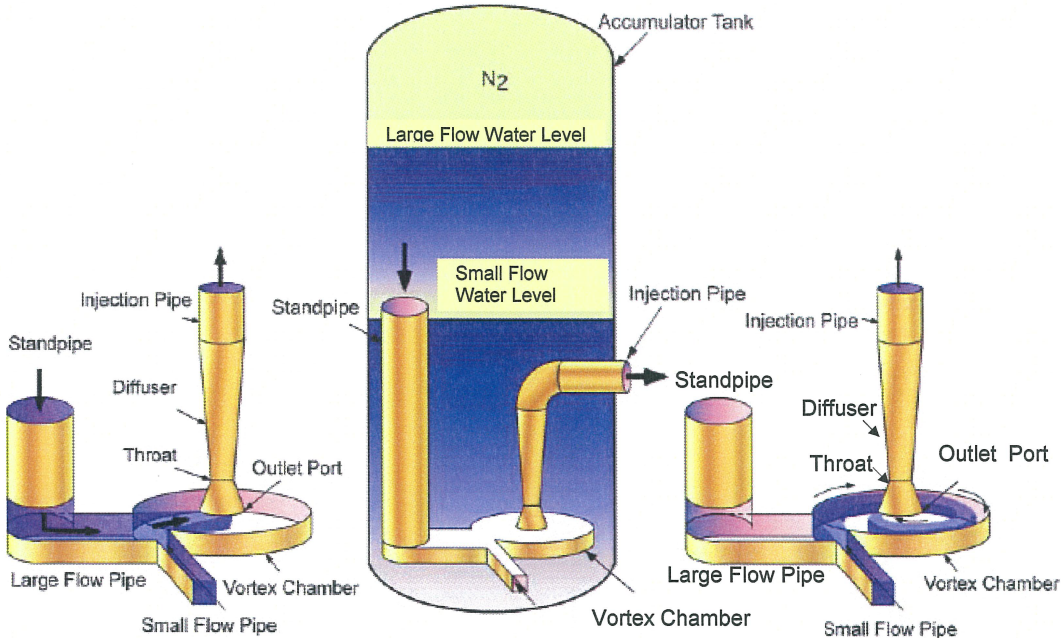

Large Flow (RV Refilling) **Water Levels in Accumulator Tank** **Small Flow (Core Reflooding)**

The vortex chamber at the inlet of the injection pipe in the accumulator accomplishes the flow rate throttling from large flow to small flow by establishing a vortex (and thus a large pressure drop) at a predetermined accumulator level. The inlet of the standpipe is located at the ACC volume level at which the transition from large to small flow is desired to occur. The ACC is a simple device that achieves precise throttling from a large injection flow rate to a small injection flow rate with no moving parts.

Upon initiation of a large break loss of coolant accident, all short term low head primary coolant injection flow requirements are satisfied by the ACC. Following depletion of the ACC water volume, the long-term ECCS flow requirements are met by the high-head safety injection pumps thus eliminating the need for low head safety injection pumps. The immediate availability of low head flow provided by the ACC upon loss of electrical power coincident with a large break loss of coolant accident provides additional time for actuation of the backup emergency power source.

The confirmatory and qualification test programs were successfully conducted. The confirmatory tests confirmed the principles of operation of the flow damper. And, the qualification testing verified that:

1. The performance of the flow damper, during large flow and small flow respectively, met the acceptance criteria (resistance coefficient for large and small flow injection)
2. Sharp flow rate switching occurred without significant gas entrainment.

Empirical flow rate coefficients have been developed from the test results and will be used in an integrated thermal hydraulic model of the US-APWR Reactor Coolant and ECCS to assure the US-APWR meets or exceeds all US safety standards.

The ACC design is expected to improve the safety of pressurized water reactors by the innovative application of the flow damper to assure the early stage of LOCA injection flow is satisfied by an inherently reliable passive system. This innovation reduces the necessity of relying on maintenance sensitive components such as low head safety injection pumps for assuring LOCA injection flow, provides additional time for actuation of backup emergency power for loss of power coincident with a large break LOCA, and reduces the net maintenance and testing burden by the elimination of low head safety injection pumps from the LOCA mitigation strategy.

8.0 REFERENCES

4.3-1 S.S. Fineblum, Vortex Diodes, pp. 48-80, Proceedings of the Fluidic State-of-the-art Symposium Held at Naval Ordnance Laboratory, White Oak, Maryland on 30 September - 3 October, 1974.

4.3-2 J. W. Stairmand, Flow patterns in vortex chambers for nuclear duties, Vol. 29, No. 6, pp. 413-418, Nucl. Energy, Dec., 1990

5-1 Mitsubishi Heavy Industries, Ltd., Large Break LOCA Code Applicability Report for US-APWR, MUAP-07011-P

5-2 Mitsubishi Heavy Industries, Ltd., Small Break LOCA Methodology for US-APWR, MUAP-07013-P

5-3 ISO/IEC Guide 98-3: 2008 Uncertainty of measurement – Part 3, Guide to the expression of uncertainty in measurement (GUM: 1995)

Appendix A

Studies on Vortex Behaviors in Flow Diodes

Flow in vortex diodes is similar to flow in the vortex chamber of the flow damper for small flow injection. Papers with regard to vortex diodes are useful to investigate the vortex behaviors for small flow injection in the vortex chamber of the flow damper. J. W. Stairmand described the flow patterns and dominant mechanisms in a vortex chamber (Ref. 4.3-2). S. S. Fineblum reported his excellent experimental results on various geometries of vortex diodes in 1974 (Ref. 4.3-1). This section provides the summaries of these reports.

1. Summary of Qualitative Investigation

J.W. Stairmand indicated that the dominant mechanism for flow in a vortex chamber is the conservation of angular momentum. In other words, he notes that the dominant mechanism for flow in a vortex chamber is the conservation of circulation. The flow pattern in a vortex chamber consists of a free vortex region in the periphery where the circulation is conserved and a forced vortex region in the central part where a significant pressure drop occurs. Therefore in the design of fluidic devices, it is important to clarify at what point the transition from free to forced vortex occurs. Stairmand used the model that was first applied to the vortex valve by Wormley. This model assumes axisymmetry and uses the momentum integral method of solving the boundary layer equations. This identifies a developing flow region ($r > r_c$) and a developed flow region ($r < r_c$). In the developing flow region, the circulation is conserved; in the developed flow region, flow is restricted by the boundary layer and the circulation is not conserved. Predictions for the distribution of swirl velocity in the vortex chamber exhibit a variety of forms to characterize the free and forced vortex modes. A modified boundary layer coefficient (BLC*) as shown below, was found to largely determine which form is taken.

$$BLC^* = \frac{2AfS^*}{Re^{*0.25}}$$

where

$$A = \frac{R}{h}$$

$$Re^* = \frac{v_i(h/2)}{\nu}$$

$$S^* = \frac{w_i}{v_i}$$

f : Friction factor for flow over the equivalent flat plate

Re^* : Reynolds number

A : Aspect ratio between the radius of the vortex chamber R and the height of the vortex chamber h

ν : Kinematic viscosity

S^* : Swirl number in the vortex chamber

v_i : The value of the radial velocity v at $r = R$

w_i : The value of the tangential velocity w at $r = R$

Wormley's theory has been used to predict the circulation distribution shown in dimensionless form in Fig. A-1. From this diagram it is clear that when BLC* is 0.25 or less, the flow in the vortex chamber conserves circulation. When BLC* is greater than 0.25, the

flow structure changes to a forced vortex at some critical radius. As BLC* is increased, the extent of this central forced vortex increases until it occupies most of the vortex chamber (BLC* = 2).

The pressure profiles across the chamber are shown in dimensionless form in Fig. A-2. For BLC* less than 1, the pressure profiles are substantially determined by inertial effects and an inviscid analysis is appropriate. Thus it seems that the viscosity effect is weak when BLC* is 1 or less.

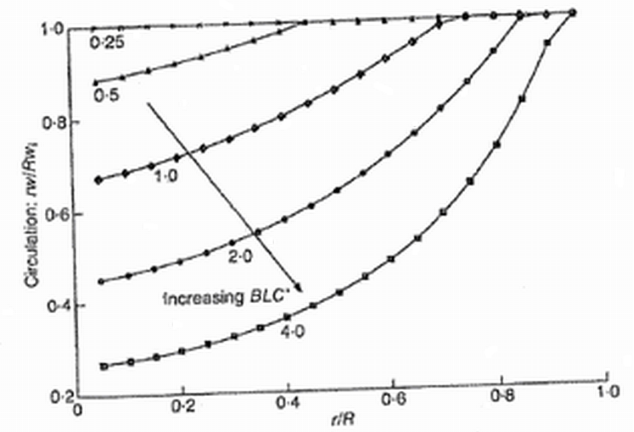

Fig. A-1 Calculated circulation distribution (Ref 4.3-2)

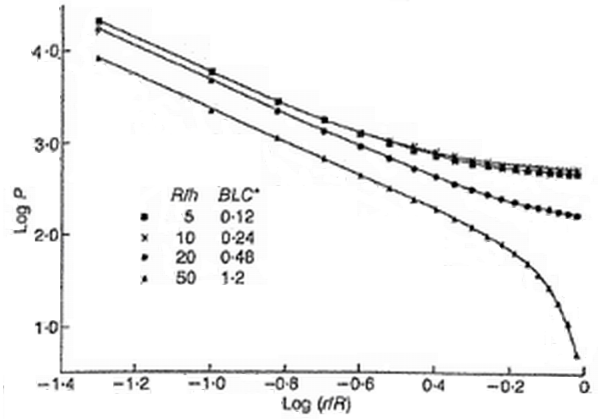

Fig.A-2 Calculated pressure profile (Ref 4.3-2)

2. Summary of Quantitative Investigations

1) Experiments

The vortex chambers used in his experiments varied in diameter, *D*, from 1.58 to 3.25 inches (40 to 82.6 mm) and in length, *L*, (equivalent to height of the vortex chamber, *H*, for the ACC) from 0.188 to 1.0 inches (4.78 to 25.4 mm). The nozzles varied in width from 0.016 to 0.4275 inches (0.4 to 11.1 mm), and the outlet varied in diameter from 0.179 to 0.394 inches (4.6 to 10.0 mm). The maximum available pressure, *p*, and flow, *Q*, were 100 psi (6.90×10^5 N/m^2) and 6 gpm (3.79×10^{-4} m^3/sec). It is not clearly mentioned in the paper, but gas or air appeared to be the working fluid because of the large tangential velocities of the diodes. If the working fluid was air at 305 K in temperature, the maximum dimensionless flow rate (equivalent to Reynolds number) $q^* = Q/(2\pi H\nu)$, is from 82 to 440. ν is the kinematic viscosity of the fluid.

2) Vortex Pressure Drop Coefficient

The pressure drop coefficient *K* is defined as:

$$K = \frac{P_o - P_i}{\frac{\rho}{2} V_N{}^2} = \frac{1}{n}\left(1 - R^{2n}\right)$$

where *R* is the ratio of the outer-to-inner radii of vortex diodes, $R=r_i/r_o$, r_i the radius of the vortex chamber, r_o the radius of the outlet port, and *n* the vortex exponent. The exponent, *n*, varies between -1 (forced vortex) and 1 (free vortex).

The tangential velocity, *V*, at an arbitral radius, *r*, is assumed to have the form:

$$V \equiv V_N \left(\frac{r_i}{r}\right)^n ,$$

where V_N is the tangential velocity from the nozzle.

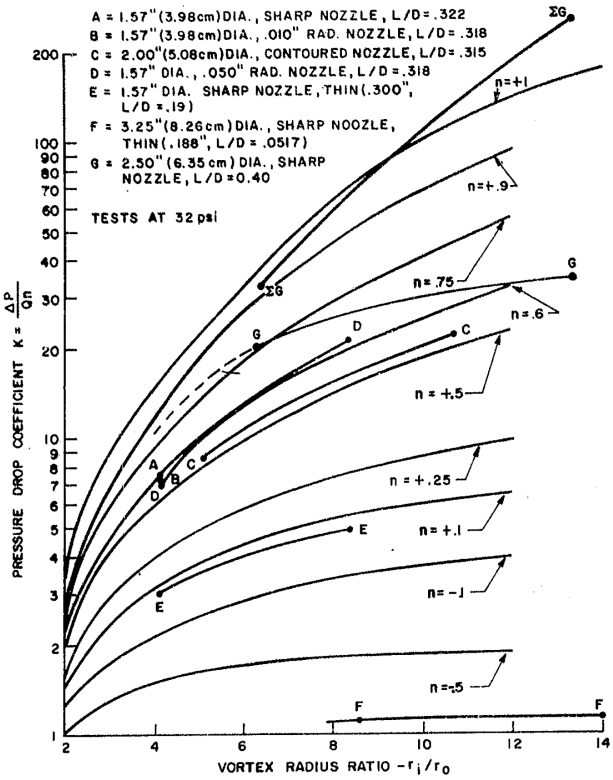

Fig. A-3 Test Results: Total Pressure Drop Coefficient across Diode Versus Radius Ratio (Ref. 4.3-1)

The variation of the pressure drop coefficient, *K*, with respect to the ratio of radii, *R*, is shown in Fig. A-3. Lines of computed *K* versus *R* with constant values *n* are plotted for comparison. The results of Fineblum show that for most vortex chambers the effective vortex exponent is approximately constant. The vortex exponent, *n*, should be chosen as an effective *n* to express the fact that many modes of flow in the vortex chamber result in a specific pressure drop and that the resulting pressure drop coefficient is a function of *R*. Therefore, *n* is an average correlation quantity rather than a true vortex exponent indicating the exact mode of vortex flow. The real flow in the vortex chamber is three dimensional due to the growth of boundary layers on the walls, which cannot be expressed by Eq. (2). Therefore, the vortex exponent "*n*" cannot be theoretically determined, but has to be experimentally determined.

3) Effect of Height-to-Diameter Ratio

For very thin diodes the boundary layers on its disk walls will completely fill the chamber. As the height increases, the available distance free of the boundary layers increases. Once this free distance is much greater than the boundary layer, further increase in L/D is not beneficial.

The average vortex exponent, *n*, increases with L/D as seen in Fig.A-4. It supports the fact mentioned above. In the cases of the vortex diodes, the vortex exponent, *n*, becomes relatively insensitive to any increase above L/D=0.35. The insensitivity limit must depend on viscosity. If viscosity effect is smaller, thickness of the boundary layer on the wall in the vortex chamber must be thinner to give a smaller insensitivity L/D limit.

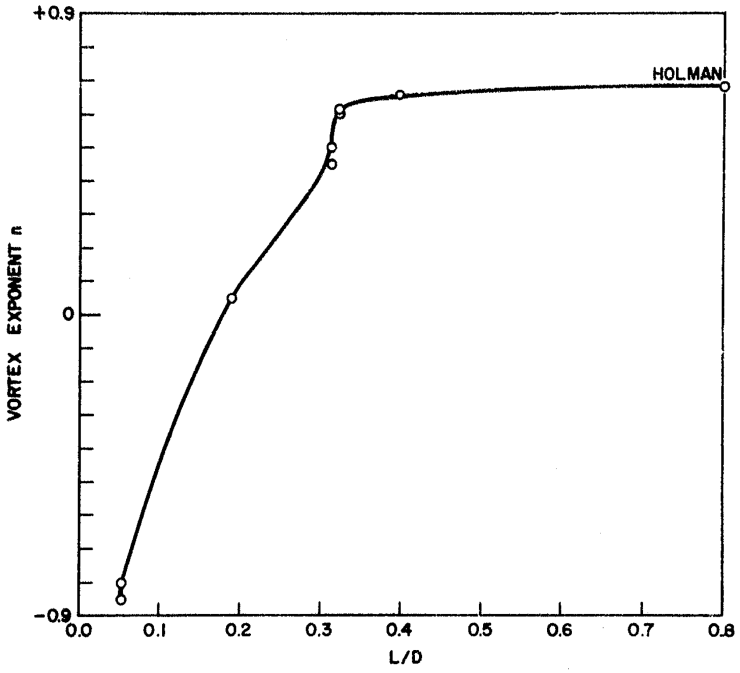

Fig. A-4 Variation of Vortex Exponent, *n*, with respect to Ratio of Vortex Height to Diameter (Ref. 4.3-1)

4) Vortex Generated Pressure Drop in Outlet Tube

Fineblum stated that, "In most cases, the pressure drop measured across the outlet tube was relatively insignificant. However, at very high values of vortex radius ratio and vortex pressure drop coefficient, the pressure drop through the outlet tube is a major portion of the total." In this case, the pressure drop in the tube immediately downstream of the vortex chamber contributes significantly to the vortex generated pressure drop. It is important to note that the swirl flow in the outlet tube originates in the vortex chamber. This means that the pressure loss from swirl flow in the outlet tube is controlled by the vortex in the vortex chamber. Strictly speaking, the dynamic pressure converted from static pressure in the vortex chamber is lost in the outlet tube, if there is no static pressure recovery.